Review

Auxetics and FEA: Modern Materials Driven by Modern Simulation Methods

Russell Galea Mifsud [1], Grace Anne Muscat [1], James N. Grima-Cornish [1], Krzysztof K. Dudek [2], Maria A. Cardona [1], Daphne Attard [1], Pierre-Sandre Farrugia [1], Ruben Gatt [1,3], Kenneth E. Evans [4] and Joseph N. Grima [1,5,*]

[1] Metamaterials Unit, Faculty of Science, University of Malta, MSD 2080 Msida, Malta;
    russell.galea.15@um.edu.mt (R.G.M.); grace.muscat.16@um.edu.mt (G.A.M.);
    james.grima.16@um.edu.mt (J.N.G.-C.); maria.cardona@um.edu.mt (M.A.C.);
    daphne.attard@um.edu.mt (D.A.); pierre-sandre.farrugia@um.edu.mt (P-S.F.); ruben.gatt@um.edu.mt (R.G.)
[2] Institute of Physics, University of Zielona Gora, ul. Szafrana 4a, 65-069 Zielona Gora, Poland;
    k.dudek@if.uz.zgora.pl
[3] Centre for Molecular Medicine and Biobanking, University of Malta, MSD 2080 Msida, Malta
[4] Department of Engineering, Faculty of Environment, Science and Economy, University of Exeter,
    North Park Road, Exeter EX4 4QF, UK; k.e.evans@exeter.ac.uk
[5] Department of Chemistry, University of Malta, MSD 2080 Msida, Malta
*   Correspondence: joseph.grima@um.edu.mt

Abstract: Auxetics are materials, metamaterials or structures which expand laterally in at least one cross-sectional plane when uniaxially stretched, that is, have a negative Poisson's ratio. Over these last decades, these systems have been studied through various methods, including simulations through finite elements analysis (FEA). This simulation tool is playing an increasingly significant role in the study of materials and structures as a result of the availability of more advanced and user-friendly commercially available software and higher computational power at more reachable costs. This review shows how, in the last three decades, FEA proved to be an essential key tool for studying auxetics, their properties, potential uses and applications. It focuses on the use of FEA in recent years for the design and optimisation of auxetic systems, for the simulation of how they behave when subjected to uniaxial stretching or compression, typically with a focus on identifying the deformation mechanism which leads to auxetic behaviour, and/or, for the simulation of their characteristics and behaviour under different circumstances such as impacts.

Keywords: auxetics; negative Poisson's ratio; metamaterials; finite elements

1. Introduction

The last three decades have seen an extensive growth in our knowledge about various new materials and metamaterials, more known as auxetics [1], which exhibit the rather unusual mechanical property of a negative Poisson's ratio [2,3]. Auxetic materials defy common expectations by expanding laterally when uniaxially stretched, rather than becoming thinner. Conversely, these materials become thinner, rather than thicker, when uniaxially compressed. In fact, the Poisson's ratio measures the magnitude of this effect [4] and is defined for a particular cross-section of a material in the plane Ox_i-Ox_j in terms of the applied strain ε_i in the direction Ox_i and the transverse strain ε_j in the orthogonal transverse direction Ox_j as

$$\nu_{ij} = -\frac{\varepsilon_j}{\varepsilon_i} \tag{1}$$

In general, for an isotropic three-dimensional (3D) material, the Poisson's ratio can assume any positive or negative value. However, for isotropic materials, this Poisson's ratio is restricted to have values $-1 \leq \nu \leq +0.5$ ($-1 \leq \nu \leq +1$ for two-dimensional (2D)

orthotropic) [5]. Materials which are auxetic in all planes for loading in any direction have been termed as "complete auxetics" whilst materials which are only auxetic in specific planes for loading in specific directions (common in crystalline materials and cubic metals [6,7]) have been termed "partially auxetic" [8–10].

Auxetics have associated with them a number of benefits and enhanced properties that are not that commonly encountered in most everyday materials [11]. They are highly desirable for their exceptional properties, including high indentation resistance [12–20], high fracture toughness [20–23], shear resistance [18,24,25], energy absorption [26,27] and other enhanced dynamic characteristics [28–31]. These unique attributes enable auxetics to find diverse applications across various fields such as in the medical field [32–37], sportswear applications [38–42], military defence equipment [43–46], as well as in the automotive [47–49] and aerospace [50–52] industries. For example, personal protective equipment (PPE) would benefit from being resistant to indentations. However, traditional materials tend to displace material away from the point of impact, resulting in reduced density upon impact. Auxetics, upon impact, behave in a manner that the material flows towards the point of impact, increasing their density and resisting indentation.

As a result of these enhanced properties and possible applications, scientists have availed themselves of various research tools to characterize, optimize and design de novo metamaterials which exhibit auxeticity. In this field of research, pure experimental research is not always deemed feasible. This may be attributed, at least in part, to the complex geometries that auxetic structures have, the lack of availability of "off the shelf" auxetic materials on a large scale, issues relating to sustainability, practical drawbacks of physical prototyping (prototypes are expensive, unsustainable, difficult to manufacture, and just a general burden to test) as well as ethical issues which may arise in certain experimental testing in real applications where auxetics could be truly needed (e.g., stents [53,54]). As a consequence, researchers have resorted to rapidly developing research protocols based on computer simulation and numerical analysis, often using experimental results and analytical studies to verify the numerical results obtained [9,55–69].

One of the numerical approaches which researchers have used to make significant inroads in the field of auxetics is the finite element method (FEM), a technique that provides an approximate solution indicating how a system behaves when subjected to specific physical constraints. The method provides easy solutions when dealing with problems involving complex geometries and/or nonhomogeneous domains having different properties in different regions. It involves the subdivision of the original domain into smaller parts called elements. The subdomains are easier to treat as they can be chosen so that their governing equations are much simpler than those for the whole domain. These elements are then connected through the nodes that they have in common. Nodes are locations in space. In general, in the case of one-dimensional (1D) elements, they would represent points on a line, while if the elements are 2D or 3D, they represent corners [70]. The shape of the elements is then determined by joining the nodes via straight lines. (Here it should be noted that sometimes elements might also have internal nodes.) Once divided into these subregions, the network of nodes is referred to as a mesh or grid. FEM then involves solving the governing equations locally at the nodes to determine the physical variables at these points. Putting together the local solutions provides a piecewise solution that represents an approximation to the actual one for the whole domain [71]. The accuracy of the solution depends on the size of the elements and increases with the number of nodes used. At the same time, the computational time increases with the number of nodes. Hence, a balance needs to be found between accuracy and processing time. Most frequently, this is established by requiring that the solution that is used does not vary by more than a small percentage (many times taken to be 1%) from that obtained using more nodes. At this point, the solution is considered to be mesh-independent. Once the FEM is applied and the solution obtained, the subsequent analysis is referred to as the finite element analysis (FEA). This method dates back to the 1940s, having been developed to overcome the mathematical difficulties when applying the theory of elasticity [72,73]. In 1956, FEA was adopted by

the aerospace industry as it allowed the modelling of complex geometries and provided instant analysis of their mechanical properties [74]. The method provided a solution to many problems of material analysis by calculating the stress within a structure [75]. The FEA method is well-known for its reliability in determining the location, magnitude, and direction of forces, as well as in assigning stresses and deformations. Therefore, within a few decades, the method was adopted by several research fields, ranging from dentistry [76–80] to biomechanics [81–84] amongst others [85–88].

A major advantage of using FEA as an integral part of a research protocol to study auxetics during the design stages is that it reduces the need for prototypes, by providing a quick, non-invasive and repeatable analysis [89–91]. Moreover, apart from the obvious sustainability advantages FEA brings with it when used for the optimization of material design whilst reducing experimental waste, FEA offers the advantage that it is an excellent tool to simulate and animate the "deformation mechanism" of auxetics, thereby providing researchers with essential information on how the deformations are leading to auxetic behaviour. This also applies to more complex systems such as 3D negative Poisson's ratio mechanical metamaterials, that are not only usually elastically stable under large compressive deformations but are also capable of exhibiting diverse properties by changing the feature size, making them potential candidates for both functional and structural applications [92]. This statement was equally relevant before the advent of 3D printing, as it is now when the current expectations regarding the performance capabilities of materials, metamaterials and structures have grown tremendously. Moreover, FEA offers the advantage that it is not limited to the conventional test parameters and can accurately and reliably simulate real-life scenarios even with unconventional parameters, such as an isotropic negative Poisson's ratio. This is particularly useful in the field of auxetics to study the behaviour of these unconventional materials in practical applications (e.g., shearing [93] or pressing [13]). Despite the lack of real materials with such properties, FEA enables us to anticipate their behaviour. Also, FEA can be used to investigate scenarios which would be difficult to achieve physically. One such study examined re-entrant hexagonal honeycombs and their post-yield behaviour under tension. Through FEA, the study revealed a plastic collapse mechanism and identified three stages of force–displacement curves [64].

FEA has been utilised in some of the earliest seminal papers on negative Poisson's ratio by Evans and his group who used the software ANSYS (Ansys Inc., Houston, TX, USA) to model two-dimensional re-entrant honeycombs as an embedded fibre in composites [94] (Figure 1a) and as a template for molecular level systems [95] (Figure 1b) to model 3D auxetic foams [96], to study continuous fibre-reinforced composites where either reinforcing or matrix constituents could have a negative Poisson's ratio [97] and to model auxetic microporous polymers [98]. Ole Sigmund [99] used a topology optimization protocol and a method based on a finite-element discretization of the base cells to propose and analyse various classical auxetic motifs. These included the double-V re-entrant system [100] and another motif [101], later referred to as the "anti-tetrachiral" motif [102–104] (Figure 1c). Nowadays, much more developed commercially available software such as ANSYS (Ansys Inc., Houston, TX, USA), MSC Marc (Hexagon AB, Newport Beach, CA, USA) and ABAQUS (Dassault Systèmes Simulia Corp., Johnston, RI, USA) combined with high computational power are essential tools when conducting research in the mechanical properties of materials and has, thus, been utilized by several research groups, as noted in Appendix A, in the study of auxetic metamaterials [63,105–113]. It is also most useful that various textbooks have been written to guide researchers through the background theory and application of FEA [70,71,114].
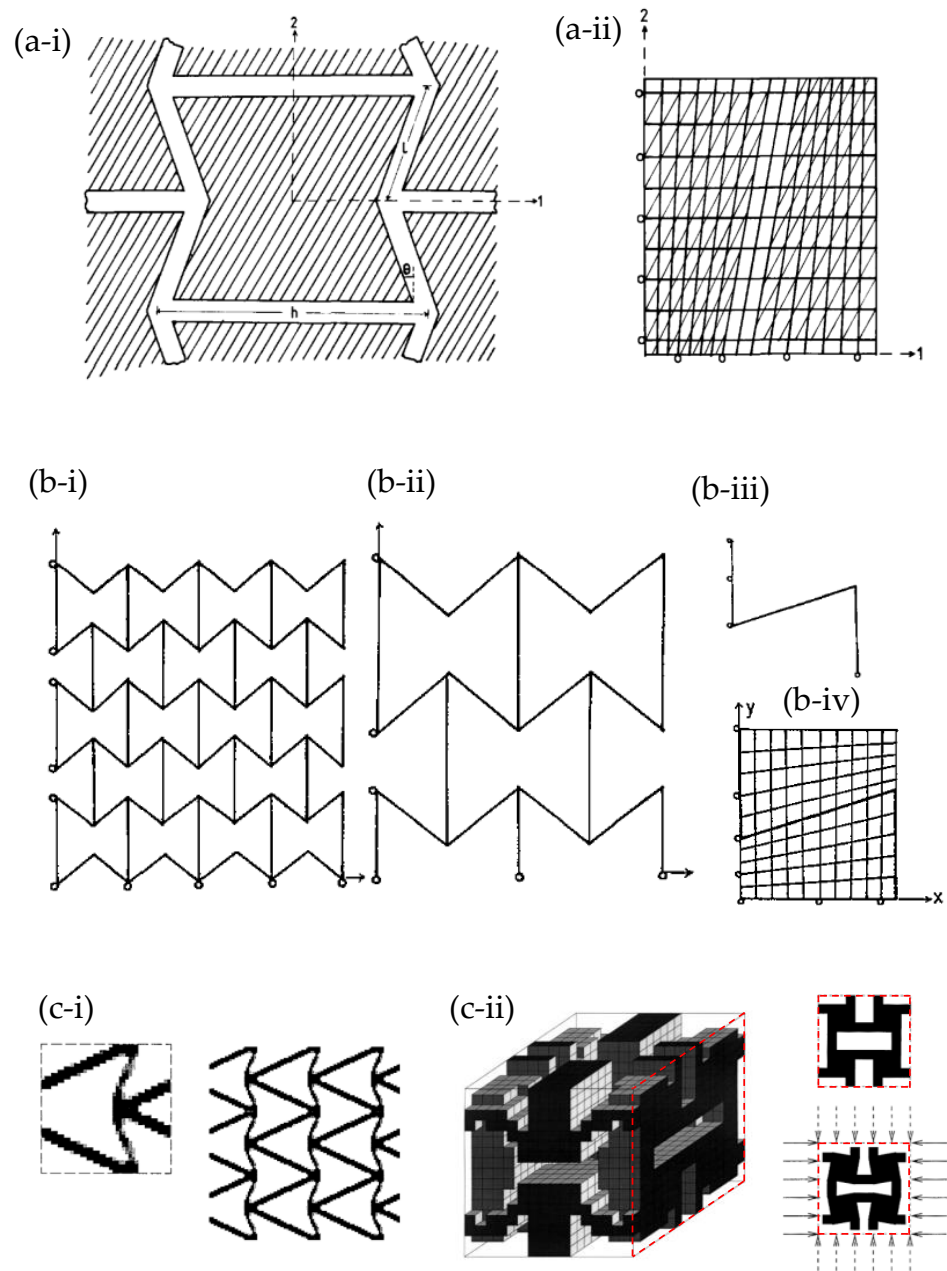
Figure 1. Some of the earliest uses of FEA to model auxetics: (**a**) Evans et al.'s (1992) matrix embedded re-entrant network-embedded fibre composite [94] with (**a-i**) showing the unit cell and (**a-ii**) showing a finite element grid used a typical re-entrant network composite with fibre re-enforcement being unshaded and matrix shaded; (**b**) various FEA representations of the analogues for the molecular level systems [95] where (**b-i**,**b-ii**,**b-iii**) correspond to systems with a different number of representative repeat units constructed from beam elements whilst (**b-iv**) represents a system where the honeycomb is embedded within an ultra-soft matrix having a near zero Young's modulus; (**c**) examples of the auxetics motifs generated by topology optimization by Sigmund, where (**c-i**) shows the double-V auxetic motif [99] and (**c-ii**) shows the motif which is now referred to as the anti-tetrachiral motif [101].

Recognizing the growth and development of auxetics, concurrently with finite element analysis, this review examines some of the major discoveries in the field of auxetics which have been made through FEA, and shows how this method of analysis contributes to the shaping of our current knowledge about negative Poisson's ratio.

2. Simulation of Auxetic Structures

The diverse range of enhanced properties associated with auxetics, together with their potential for use in several practical applications meant that, in the last four decades, considerable effort has been made to design and develop novel or improved auxetic structures. In fact, as clearly stated by [115], there is a constant "demand for new types of auxetic structures to achieve different design goals of their use (dynamic behaviour, fatigue resistance, manufacturability)".

If one had to look at the modus operandi which has been used to generate and optimise auxetics, one can clearly identify various approaches, including what may be referred to as the "systematic geometry-based approach" and the "topology optimisation approach". The former approach may be explained through the specific example of the 2D re-entrant geometry motif shown in Figure 1a, which has long been recognised for its potential as an auxetic system [1,116,117]. The systematic approach typically starts with the identification of geometric parameters which characterise the system, in this case, the length of the slanting ligament (l), the length of the ligaments connecting them (h) and the angle between them (θ). It then examines how each of these parameters, and/or combinations of them, affects Poisson's ratio. This can be achieved through, for example, the formulation of analytical models based on assumptions of how the systems deform (e.g., flexure, hinging and/or stretching of the ligaments) and/or running a series of FEA simulations where each parameter is varied whilst keeping the other parameters fixed. Both the analytical and simulation approaches offer distinct advantages and disadvantages. Analytical models lead to mathematical expressions for Poisson's ratio in terms of geometric parameters. On the other hand, the systematic FEA approach allows for a more realistic representation of systems, as discussed elsewhere [118]. The topology optimisation approach, first applied and pioneered in the field of auxetics in the 1990s by Sigmund and co-workers [100,119,120], has the capability of automatically achieving an optimal structure and material layout (geometry) with a negative Poisson's ratio subject to specific pre-defined constraints through the use of advanced algorithms. [115,121] Such constraints include the desired macroscopic properties and prescribed performance. For example, this approach can help identify optimal structural configurations that maximize the desired properties of auxetic materials, such as impact resistance or energy absorption, while maintaining or reducing material weight. Typically, the optimised structures obtained have their properties evaluated through FEA before potentially being manufactured as prototypes for experimental testing [122,123]. Various studies have applied the technique within the field of auxetics, including a study by Clausen et al. [124] who employed parameterized optimization to produce auxetic chiral topologies which maintain their desired Poisson's ratio over strains; a study by Bruggi et al. [125] who made use of SIMP-based topology optimization (i.e., solid isotropic material with penalization) to obtain auxetics based on micropolar materials; and a study by Wang et al. [126] who applied isogeometric topology optimization with the aim of reducing stress concentrations within star-shaped auxetic structures.

2.1. Two Dimensional Systems

A substantial number of studies on auxeticity were devoted to investigating the mechanical properties of two-dimensional motifs that are capable of exhibiting a negative Poisson's ratio. This focus on 2D systems is probably due to the fact that the Poisson's ratio v_{ij} can essentially be regarded as a 2D property.

The re-entrant honeycomb geometry, shown in Figure 1, is one of the most studied auxetic motifs. This structure essentially represents a standard hexagonal honeycomb where the classical Y-shaped joints have been inverted to form arrow-shaped joints. Such systems are known to exhibit a negative Poisson's ratio when loaded on-axis, primarily due to flexure (or hinging) of the slanting ligaments. This motif, equally useful as a 2D system and as a model for particular cross-sections of 3D materials, was one of the earliest auxetic systems studied by FEA around three decades ago [94–96] (Figure 1a,b). Since then, numer-

ous modified re-entrant structures were tested through FEA to diversify and/or optimise the geometry [127–129] and to analyse the resulting mechanical properties such as energy absorption capacity [127], synclastic behaviour [130,131] and impact resistance [132–134].

Numerous other studies have utilised FEA to investigate several variations based on the 2D re-entrant hexagonal honeycomb systems and Sigmund's double-V model (Figure 1c-i) to simulate their mechanical properties, including in-plane Poisson's ratio and Young's modulus under uniaxial loading [135–139]. Through FEA simulations, several studies were carried out on the shape optimization of the re-entrant honeycombs by analysing the effect of a number of variables on the physical properties. For instance, Lu et al. in 2016 [140] analysed a re-entrant honeycomb with an additional narrow rib in the unit cell, resulting in a cellular structure with significantly enhanced Young's modulus [140]. Bezazi et al. in 2005 [135], and the subsequent work by Harkati et al. in 2017 [128], investigated the system illustrated in Figure 2b. Most notably, Bezazi et al. reported that for certain internal angles, the proposed structure exhibits a decrease in the Poisson's ratio when compared to the conventional honeycomb. Also, the presence of edge corners in the proposed configuration gives rise to a cellular structure with enhanced flexibility compared to the classical centrosymmetric one [135]. In the follow-up work, Harkati et al. [128] investigated the shear and axial deformation using FEA, providing a better insight into the deformation mechanism for the auxetic behaviour and the geometric parameters governing them, specifically the cell wall thickness [128]. Moreover, Gohar et al. [127] used FEA to optimize and model various novel auxetic structures under compressive loading (Figure 2c), systems which they then constructed using 3D printing and tested physically. These included a set of novel re-entrant structures, termed mixed-star structures. These re-entrant structures exhibited a number of superior properties, including a high energy absorption capacity [127].
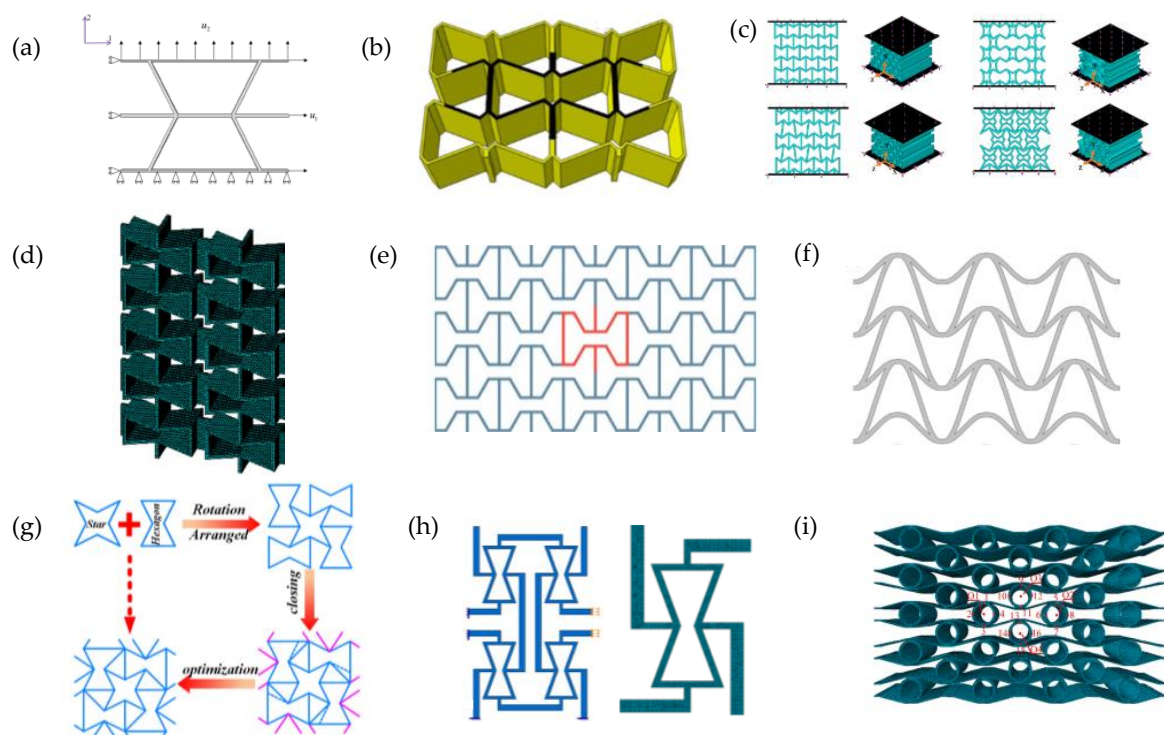
Figure 2. Examples of modified re-entrant structures, which can be seen as variations in the units in Figure 1, proposed by (**a**) Lu et al. (2016) [140]; (**b**) Bezazi et al. (2005) [135] and Harkati et al. (2017) [128]; (**c**) Gohar et al. (2021) [127]; (**d**) Huang et al. (2017) [141]; (**e**) Khan et al. (2019) [59] and Mustahsan et al. (2022) [142]; (**f**) Guo et al. (2020) [143]; (**g**) Wang et al. (2023) [144]; and (**h**) Zhang et al. (2021) [145] and (**i**) Li et al. (2022) [129].

Similarly, Huang et al. [141] investigated a new type of honeycomb design consisting of two distinct parts, a re-entrant hexagonal component, and a thin plate section, illustrated in Figure 2d. The authors developed theoretical models describing the in-plane uniaxial tensile modulus, shear modulus and Poisson's ratios, and verified them through FEA [141]. FEA was also instrumental in validating analytical and experimental methods, as demonstrated in the work by Khan et al. [59] and Mustahsan et al. [142] (Figure 2e). These used FEA in conjunction with experimental testing to validate the analytical model accounting for the bending, shearing and axial deformation of modified re-entrant honeycomb structures and showed a close agreement between the three methods (numerical, analytical and experimental). Other notable studies include the investigations by Guo et al. (2020) [143] on the double-U honeycomb structure shown in Figure 2f, in which the arrow-shaped system in Figure 1c-i proposed in the 1990s by Ole Sigmund [99] and Larsen et al. [100] was modified to have better load resistance and a higher energy absorbing capacity [143], and the WSH honeycombs composed of stars and hexagons studied by Wang et al. (2023) (Figure 2g) which exhibited excellent energy absorption capacity and enhanced anti-impact behaviour [144].

Another study carried out by Zhang et al. investigated two new hybrid metamaterial concepts combining a core unit cell of re-entrant or cross-chiral shape with lateral missing ribs (Figure 2h). FEA simulations optimised specific effective properties, while non-linear simulations were used to study the Poisson's ratio and stiffness of these metamaterials under large deformations [145]. Similarly, Li et al. proposed the composite auxetic structure consisting of corrugated sheets and tubes, shown in Figure 2i. This was studied using FEA, in conjunction with experiments and theoretical analysis, to investigate the variables affecting the Poisson's ratio and the mechanical properties of the structure, as well as shape optimization [129]. Other rather complex 2D systems studied include the hierarchical re-entrant honeycombs by Zhan et al. (2022), who used FEA to show that these systems exhibit enhanced mechanical properties under compression. Here, analysis of the deformation shows that when the system is compressed, the addition of a second order triangular hierarchy converts the deformation mechanism from bending-dominated to stretching-dominated, and revealed a combination of deformation mechanisms which contributed to significant improvement in the mechanical properties [146].

The FEA method has been employed to explore various other auxetic mechanisms including chiral systems and rotating rigid units. In particular, inspired by work the of Lakes [147,148] and Sigmund et al. [101], FEA was a key tool in studying 2D periodic systems characterised by highly ordered chiral sub-units [102–104,129,149–157] (such as the ones in Figure 3a,c), as well as systems with disordered or irregular chirals [158,159] (such as the system in Figure 3c).

Here, FEA was used to carry out parametric studies to optimise the geometries of the proposed chiral systems and to investigate their mechanical properties such as auxeticity, energy absorption capacity, shear resistance and much more. The unifying design aspect of these chiral systems is that they generally consist of rigid nodes to which thin flexible ligaments are attached in a manner that they form a chiral building block. As discussed by Alderson et al. [104], to model this system through a representative volume unit, it is essential to apply the appropriate boundary conditions and constraints (see Figure 3a-iii,a-iv as an illustration of typical constraints applied). Furthermore, as highlighted by Mizzi et al. [160], the correct application of the boundary conditions often dictates the success or otherwise of a simulation. Simulations of systems with a chiral building block such as the ones shown in Figure 3a–c demonstrate that auxeticity from the "chiral mechanism" occurs when the ligaments are flexible and the nodes are rigid. Generally, when the system is subjected to uniaxial compression, the nodes with the ligaments attached to it rotate, thus, constraining the ligaments to flex in synchrony (to some extent or another). This synchronized mode of deformation causes a lateral contraction which in turn results in auxeticity, something which is even evident in the irregular hexachirals simulated by FEA by Mizzi et al. (2018). [159] However, when the nodes are much less

rigid than the ligaments, deformations occur predominantly in the nodes, as demonstrated by Attard et al. (see Figure 3c-ii) [150]. The authors referred to this mechanism as the "starchirals mechanism".

FEA was also one of the main tools used to explore how slits and perforations could generate a negative Poisson's ratio [161–167]. Notably, early studies on this idea (Figure 4a–c) highlight how strategically placed perforations could transform a regular sheet to an auxetic or zero-Poisson's ratio system by making it mimic the "rotating squares" [168] and "rotating triangles" [169] auxetic mechanisms. This could be achieved when using appropriately placed diamond-shaped (Figure 4a) [161], slit [162] (Figure 4d), star-shaped [164] (Figure 4b) or triangular-shaped [164] (Figure 4c) perforations. Other similar studies investigated the mechanical properties and deformation mechanisms of "rotating rigid units"-mimicking systems. Amongst others, Wang et al. (2021) [170] and Atilla Yolcu et al. (2022) [171] explored such systems designed through the use of regularly and irregularly peanut-shaped perforations (depicted in Figure 4e); Acuna et al. [172] simulated rectangular perforations; whilst Mrozek and Strek [173] (Figure 4f) investigated a system of perforations mimicking the rotating squares model [64,174–176]. Afshar et al. utilised FEA to investigate non-porous perforated rotating rigid units having a soft inclusion in the perforations. It was shown that these inclusions still retained a negative Poisson's ratio but reduced the extent of auxeticity. This would be useful in applications of non-porous auxetic materials [105]. Similar conclusions were also drawn in an earlier FEA study by Mizzi et al. (2015) [177] which examined non-porous grooved single-material systems.
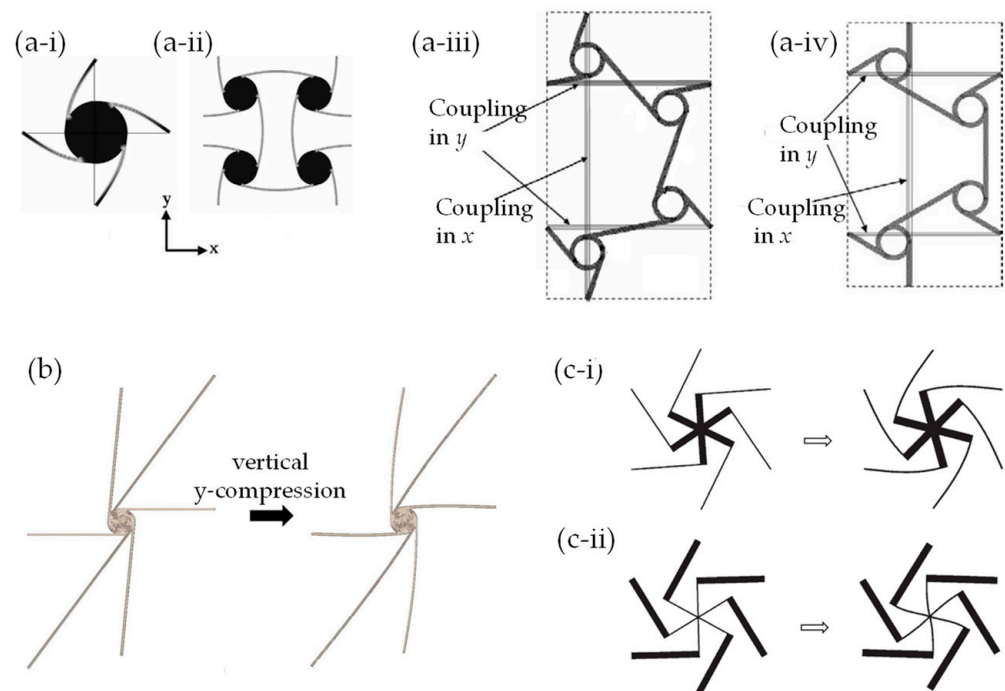

Figure 3. Examples of auxetics with chiral building blocks or based on rotating rigid units obtained via slits or perforations: (**a**) the repeat units in the regular (**a-i**) tetrachiral, (**a-ii**) anti-tetrachiral (**a-iii**) trichiral and (**a-iv**) anti-trichiral, as presented in the work by Alderson et al. (2010) [104]; (**b**) the repeat unit and the manner it deforms as predicted by FEA of an irregular hexachiral [159]; (**c**) FEA-simulated deformations of uniaxial compression in the vertical y-direction of (**c-i**) hexachirals, where the star-shaped node is much more rigid than the ligaments, and (**c-ii**) starchirals, where the ligaments are much more rigid than the nodes with the consequence that deformations occur within the nodes (the "starchiral mechanism") [150].
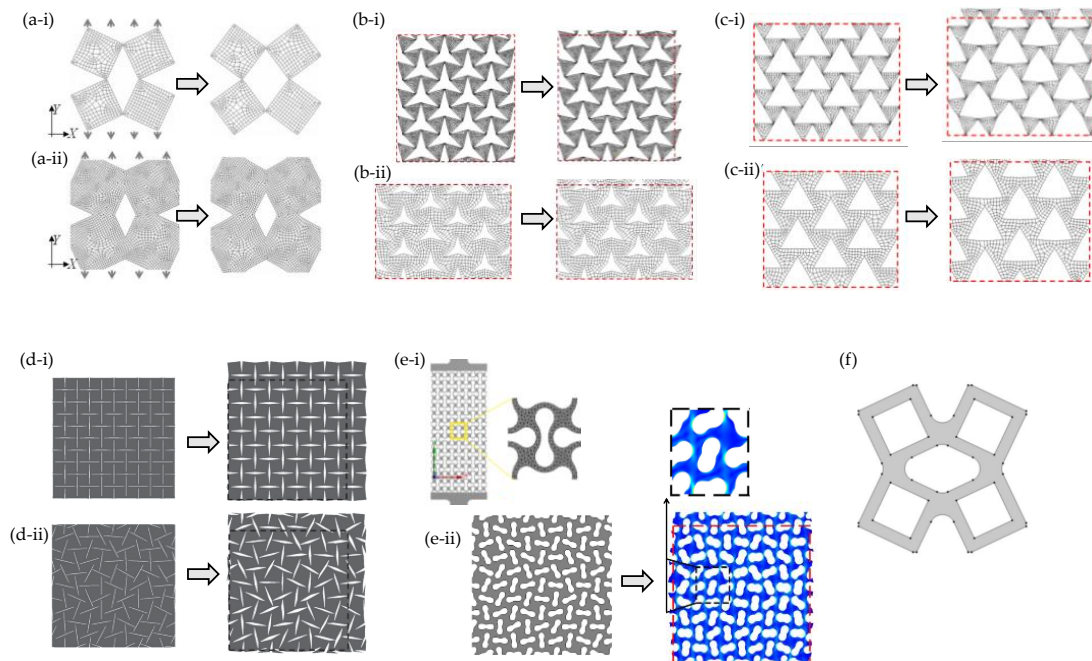
Figure 4. Examples of perforated systems which mimic rotating rigid units: (**a**) systems with diamond-shaped perforations where system in (**a-i**) has minimal overlap compared to system in (**a-ii**); (**b**) systems with star-shaped perforations where system in (**b-i**) has minimal overlap compared to system in (**b-ii**); (**c**) systems with triangle-shaped perforations, where system in (**c-i**) has minimal overlap compared to system in (**c-ii**); (**d**) systems with slits (regular (**d-i**) and randomly oriented (**d-ii**)); (**e**) system with (**e-i**) regularly and (**e-ii**) irregularly placed peanut-shaped perforations; and (**f**) implementation of a rotating squares model as proposed by Mrozek and Strek et al. (2022) [173]. Systems in (**a,d,e,f**) mimic the rotating squares model, whilst (**b,c**) mimic the rotating triangles model. Note that, if applicable, systems are being loaded vertically.

2.2. Three Dimensional Systems

3D auxetic materials and models, ranging from crystalline materials such as zeolites, silicates, etc. [178–180] to macroscopic systems such as the Hoberman sphere [181] are gaining importance due to their abundance, versatility, properties and potential applications. However, their added complexity compared to their 2D counterparts, can make the interpretation of their Poisson's ratio more challenging. In 3D auxetics, the overall deformations might result from multiple auxetic mechanisms acting simultaneously, as evident in some of the earliest seminal work in the field (Figure 1c-ii) [101]. FEA, thus, becomes an even more indispensable tool to elucidate their intricate behaviour. In fact, FEA has been extensively used to investigate a wide range of 3D auxetics including cellular materials [129,171,182], composites [183–187] and some rather novel constructs such as a surface auxetic structure (SAS) [188].

FEA has offered diverse insights into the effects of different geometric parameters on the mechanical properties and deformation mechanisms in 3D systems from as early as the 1990s. The diversity of systems studied can be appreciated from some cellular systems shown in Figure 5. Evans et al. [96] used the elongated dodecahedron as a model for auxetic foams (Figure 5a). More recently, Yang et al. [189] and Wang et. al. [190,191] studied a 3D re-entrant honeycomb (Figure 5b); Nasim and Etemadi [192] proposed a cellular structure (Figure 5c); Farrugia et al. (2019) [193] explored a novel 3D anti-tetrachiral honeycomb Figure 5d; and Wang et al. (2020) [194] investigated "3D cross-chiral auxetic materials", a system where some of its 2D projections bear a very close resemblance to the "rotating squares" [168] profile with the squares replaced by crosses [195] (Figure 5e). Later, in 2021, Photiou et al. worked on the so-called "tetra-petal auxetic [196] (Figure 5f), while in 2022, Grima-Cornish et al. [197] examined the crystalline material framework of boron

arsenate as if it were a purely mechanical system (Figure 5g). Recently, it has also been proposed that 3D auxetic systems may be constructed by introducing continuous voids having constant cross-sectional areas at particular loci in different planes [198]. Collectively, these works highlight how FEA simulations have become the staple tool to bridge design and mathematical modelling with experimental work and physical testing. Moreover, for a given idealised design or concept, FEA has made it possible to obtain a glimpse into how real systems might behave, thereby guiding experimentalists towards the synthesis of systems with tailor-made auxetic properties. All this contributed significantly to the growth of the field of auxetics over the last decades. While most 3D cellular systems exhibit their auxetic behaviour through "re-entrant" or "rotating rigid units" (or its chiral variant) mechanisms, Su et. al. investigated a 3D-printable auxetic metamaterial operating through a sliding mechanism (Figure 5h). Their experimental and FEA simulations produced coherent results, and the proposed structure was claimed to exhibit superior performance to the 3D re-entrant honeycomb, due to higher compression resistance and more stable auxetic behaviour [199].
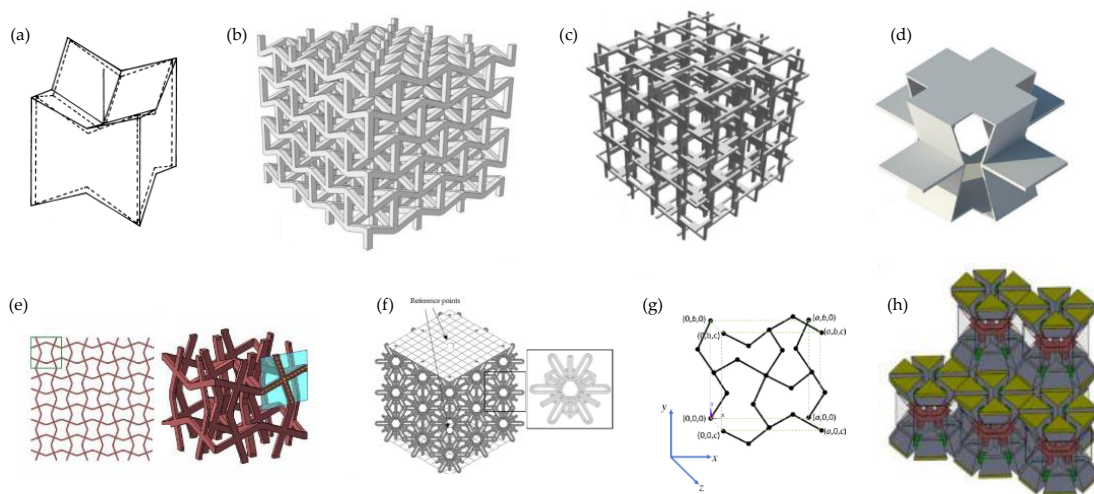

Figure 5. Examples of 3D cellular structures studied via FEA in the last three decades: (**a**) work by Evans, Nkansah and Hutchinson, 1994, on a cellular systems to simulate the microstructure of auxetic foams [96]; (**b**) work by Wang et al., 2017, on a re-entrant version of the classical re-entrant honeycomb [191]; (**c**) another 3D version of the re-entrant honeycomb as studied by Nasim and Etemadi, 2018 [192]; (**d**) the 3D chiral cellular structure as proposed and studied by Farrugia, Gatt and Grima, 2019 [193]; (**e**) a 3D cellular system as studied by Wang et al., 2020, which can be seen as a 3D render on the "rotating squares" [194]; (**f**) a 3D cellular structure proposed, modelled and tested experimentally by Photiou et al., 2021 [196]; (**g**) a mechanical version of a crystalline system modelled by Grima Cornish et al., 2022 [197]; and (**h**) a sliding system investigated by Su et. al. (2021) [199].

From a design and modelling perspective, the possibility to make use of the third dimension brings with it some very interesting possibilities on how to achieve auxeticity. FEA facilitates the transition from concept to an actual physical model. Thus, tubular structures were made by morphing novel or existing 2D auxetics into the shape of a tube for potential use as biomedical devices like artery stents. Wu et al. (2018) [62] (Figure 6a-i) followed the design principles proposed by Gatt et al. [200] (Figure 6a-ii) to explore the mechanical properties of the proposed artery stents. Understanding such properties is crucial for the mechanical integrity and biomechanical performance reliability of the stent–plaque–artery system. Wu et al. proposed two innovative chiral stent types with auxetic properties: an anti-tetrachiral stent with circular and elliptical nodes, and a hierarchical anti-tetrachiral stent with circular and elliptical nodes (Figure 6a). FEA was employed to study the effects of stent geometrical parameters on the tensile mechanical behaviour of the proposed stents. It was deduced that the proposed anti-tetrachiral stent can be tailored by adjusting the levels of hierarchical structures and unit cell design parameters. FEA

was used to study the deformation mechanism during stenting. The proposed structures exhibited remarkable radial expanding abilities while maintaining axial stability, which is ideal for such applications [62].
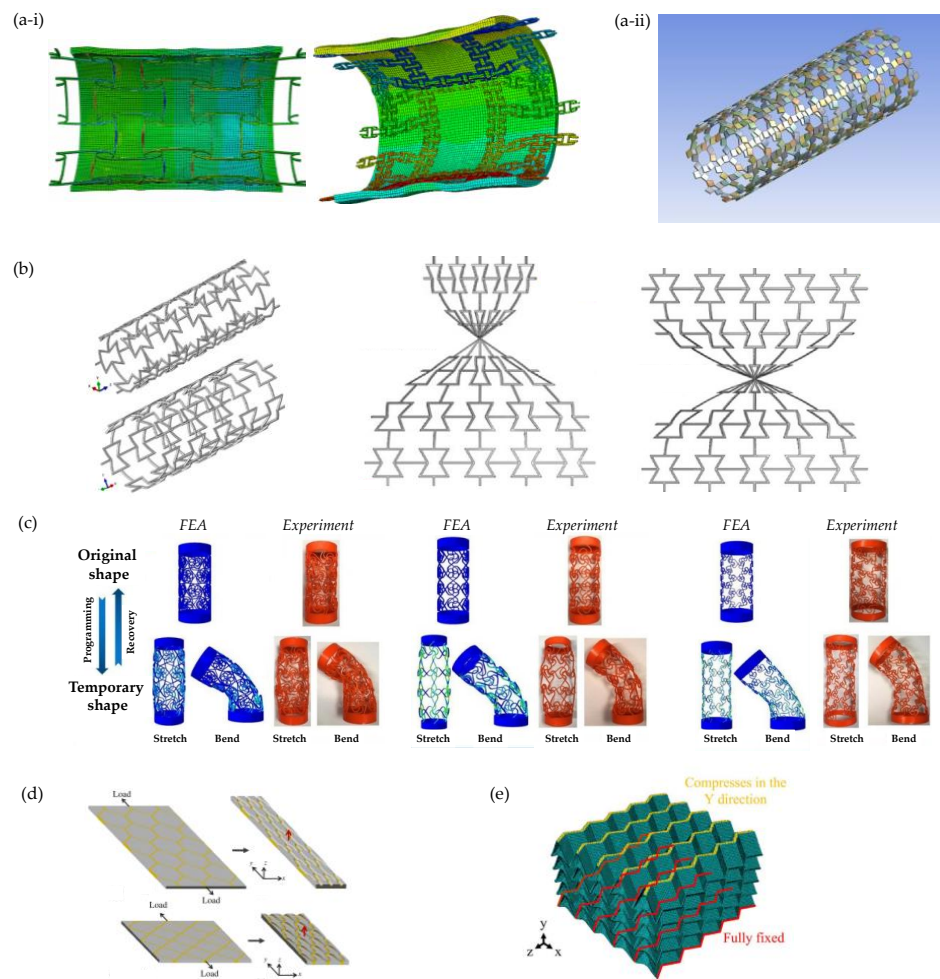

Figure 6. Other examples of 3D auxetics studied via FEA: (**a**) simulations by Wu et al. [62] of the mechanical properties of (**a-i**) regular and hierarchical anti-tetrachiral auxetic stents, the latter being based on the design concept by Gatt et al. [200] shown in (**a-ii**); (**b**) 2022 work by Changfang et al. [188] on surface auxetic structures; (**c**) 2022 work by Wan et al. [201] on programmable auxetic metamaterials with shape memory effects; (**d**) honeycomb composites with auxetic out-of-plane characteristics as proposed and modelled by Grima et al. [183]; and (**e**) 2023 work by Li et al. [187] on the auxetic and failure characteristics of composite stacked origami cellular materials under compression.

Other studies of this type include work on the surface auxetic structures (SAS) studied by Changfang et al. (2022) [188] (Figure 6b). These structures are obtained by morphing 2D auxetic surfaces into 3D shells. FEA was employed to study two types of SAS: RAS (reversed auxetic structure) and CAS (crimped auxetic structure). The focus was on simulating the compressive behaviour of both plane and surface auxetic structures to understand their mechanical behaviour and energy absorption characteristics. Through this study, it was deduced that RAS displayed the auxetic effect of compression shrinkage as well as the super-mechanical effect of compression twist. Such behaviour was found to appear only in the local positions of the beams, giving the structure great potential in engineering applications [188]. Recent work by Wan et al. delved into four-dimensional (4D) printed programmable auxetic metamaterials with shape memory effects, using both FEA (see Figure 6c) and experimental approaches [201]. The analysis revealed that the proposed

cylindrical shells possess desired mechanical properties and configurations, indicating potential applications as biomedical scaffolds [201].

FEA has also proven particularly valuable when analysing auxetic composite structures. This is evident from the early contributions to the field by Evans et al. [94,97]. Grima and co-workers [183] used FEA simulations to demonstrate how an auxetic 3D composite consisting of metal honeycombs embedded in a soft rubbery matrix could exhibit a negative Poisson's ratio out-of-plane by forcing the softer matrix to move out of the pores whilst the honeycomb is stretched (Figure 6a). Through FEA, researchers could investigate the effects of changes in framework geometry in relation to changes in the Poisson's ratio both in-plane and out-of-plane. This enabled the optimisation of composite parameters for maximum auxetic behaviour [183]. Additionally, these simulations led to an analytical study outlining the requirements for auxetic behaviour.

Recent work on composites also includes that of Li et. al. (2023) [187] who used FEA to investigate the mechanical and auxetic characteristics of a composite fibre-reinforced stacked origami structure (Figure 6d). It was deduced that composite stacked origami structures have lower density and better energy absorption characteristics compared to those made from metal using additive manufacturing processing [187]. Another interesting work is that on cementitious composites [184], where FEA-based machine learning was used to generate accurate predictions of the auxetic behaviour in cementitious composites [184].

3. Simulation of Responses on Auxetics under Dynamic, Quasi-Static Loading, Impact and Indent Loading

The use of FEA as a tool to simulate the responses of auxetic materials and structures has been pivotal, primarily due to its efficiency and time/cost-effectiveness compared to actual physical testing as it reduces the need for production and testing of experimental prototypes [192,202]. FEA's efficiency lies in its ability to accurately acquire the desired mechanical responses and to analyse the behaviour of different sections of the material in a manner which is sometimes difficult to perform experimentally in a non-destructive manner. This is crucial when assessing the response of the material to applied loads and other desirable properties as required by the intended application.

The properties of auxetics are inherently linked to their geometry (including topology) and deformation mechanism (which may be controlled through a number of ways, such as materials contrast [203]). To achieve the desired properties, researchers often investigate the effect of the geometric parameters on the mechanical properties and behaviour of auxetics under specific conditions. Recently, there has been growing interest in the mechanical properties and energy absorption capacity of auxetic materials under dynamic and quasi-static loading. One of the key challenges in this area is to develop a deeper understanding of the factors that influence these properties under different loading conditions and the deformation modes of specific auxetic structures, challenges which may be successfully addressed using FEA.

In a 2022 study, Han et al. [204] used FEA to investigate the mechanical properties and deformation modes of gradient and uniform auxetic tubes subjected to axial and inclined loads (Figure 7a). Their findings revealed that the gradient auxetic tube had better energy absorption capacity and higher strength compared to the uniform auxetic tube [204]. Similarly, in the same year, Han, Ren et al. used FEA to investigate a design for ribbed metamaterials with high-quality energy-absorption capability speeds [205]. In a more recent study, Wang et al. [144] conducted numerical simulations to study the static and dynamic plateau stresses of windmill-like (WSH) honeycombs and their energy absorption capacity (Figure 7b). Comparing these with the STAR-4 auxetic honeycomb and the standard re-entrant honeycombs, they found that the windmill-like (WSH) honeycombs had excellent energy absorption performance under both static and dynamic loading conditions [144]. In the study by Chen et al., a set of auxetic lattices with enhanced stiffness were proposed. This was achieved by adding a strengthening rib into conventional auxetic unit cells in a direction perpendicular to the re-entrant direction. The effective

mechanical properties of these variants were calculated using the fast Fourier transform-based homogenization method, which illustrated that their Young's modulus in 2D can be improved by approximately 200% along the strengthening direction without significantly sacrificing the auxetic characteristics. However, such an enhancement is weakened in 3D. The paper provides insight into the design of the new structures of unit cells with enhanced stiffness and a negative Poisson's ratio [206].
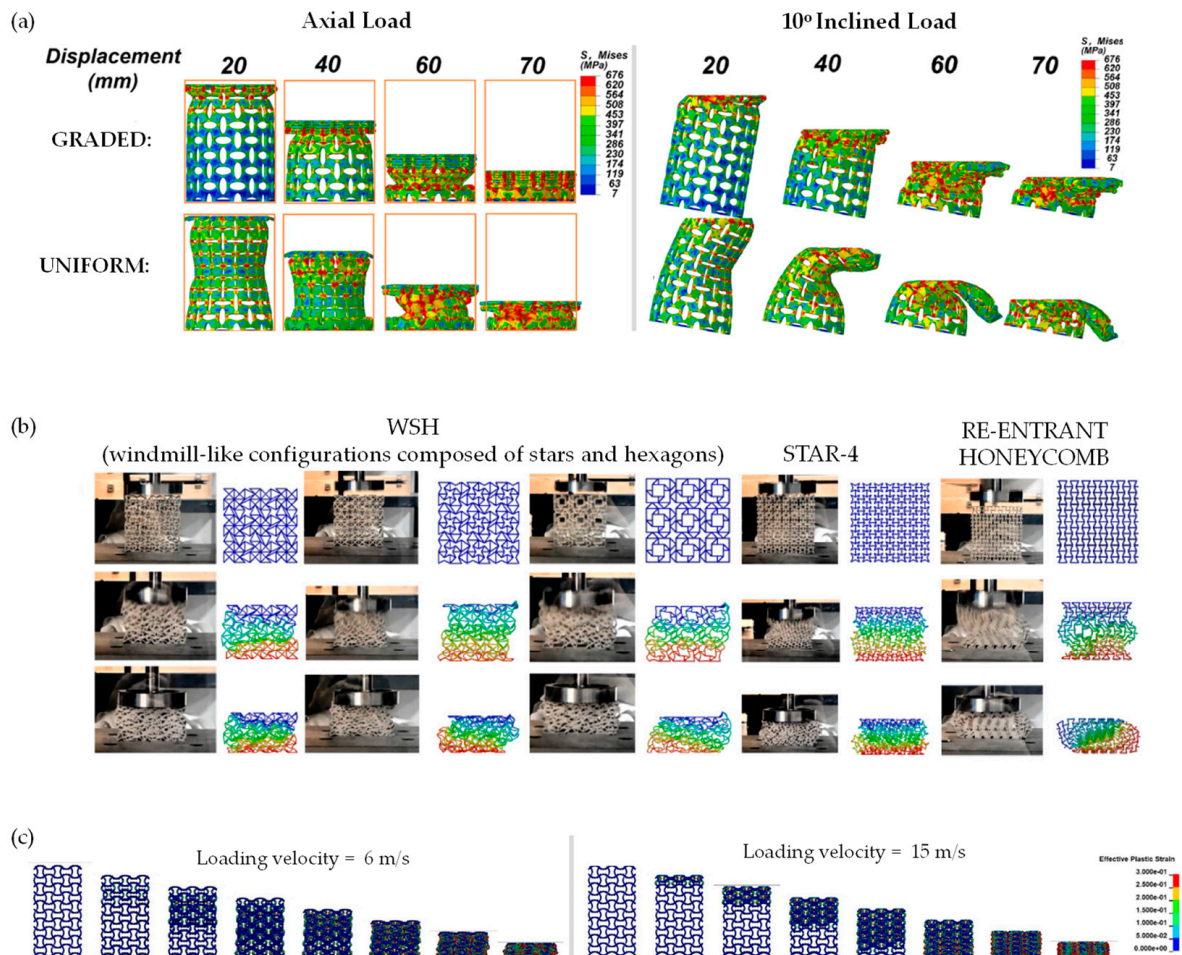

Figure 7. Examples of dynamic simulations: (**a**) deformation modes of a gradient auxetic tube and uniform auxetic tube under axial and inclined loads for 3D auxetics studied via FEA by Han et al.'s 2022 work [204]; (**b**) work by Wang et al. (2023) showing a comparison of experimental and FEA deformation diagrams under dynamic impact behaviour with an impact velocity of 1.7 m/s [144]; and (**c**) uniaxial compression at different velocities of the regular chiral as simulated by Novak et al. [207].

Novak et al. [18,207] explored the mechanical behaviour of chiral auxetic [207] (see Figure 7c for the results of the simulation of a regular chiral auxetic under dynamic uniaxial compression at different velocities) and graded/non-graded [18] cellular structures under different loading conditions. Their investigation included quasi-static low-velocity dynamic compression and high-strain rate loading and shearing scenarios. The study employed experimental measurements, infrared thermography, high-speed camera images and computational simulations to examine the deformation mechanism of chiral auxetic structures. Computational simulations were used to obtain a more detailed analysis of mechanical behaviour at different strain rates and estimations of plateau stress at arbitrary loading velocities. As a result of this analysis, Novak et al.'s work provides insights into the use of chiral auxetic structures in crashworthiness, ballistics and blast protection applications [18,207].

Other noteworthy studies that have made use of dynamic and quasi-static compression, as well as different impact velocities, include several modified re-entrant diamond structures which exhibited a superior specific energy absorption [208,209]. Similarly, investigations of modified re-entrant honeycombs exhibited potential for crashworthiness applications [210,211]. Additionally, studies examining the energy absorption capacity of star-circle honeycomb structures led to the development of different design strategies for the auxetic honeycomb [212].

FEA has also been implemented to expose such materials to dynamic and static crushing conditions. Li et al. conducted a study to analyse the in-plane uniaxial and biaxial crushing characteristics of three honeycombs through explicit dynamic FEA. This research aimed to compare the deformation mode, plateau stress, energy absorption and impact response [213]. In a 2019 study by Qi et al. [154], the in-plane crushing response of tetrachiral honeycombs was investigated under both quasi-static and dynamic loading conditions. This revealed the different modes of deformation in response to the different loading conditions [154] (Figure 8a). A subsequent study by the same authors [214] (Figure 8b) made use of the FEA-predicted deformation to reveal the underlying mechanisms by analysing patterns in the internal stresses for a re-entrant honeycomb with petal-shaped inclined ribs, which they termed as "re-entrant circular auxetic honeycombs". The article identifies three distinctive regions in their unit cell configuration map, each corresponding to a mesoscale interaction pattern and a macro-scale deformation mode [214].

Other studies analysing the crushing performance through FEA include a paper published in 2020 by Wei et al. [215] investigating the deformation upon the crushing of star-shaped honeycombs and a new type of auxetic honeycomb "star" structure (termed star-triangular honeycombs) (Figure 8c). Another study by Singh et al. [216] used FEA to investigate the deformation mechanisms observed during the static inclined compression of the re-entrant honeycomb auxetic structure (Figure 8d), a mode of loading which is likely to have a number of practical applications. This research introduced a novel method to extract micro deformation mechanisms under inclined loading, which were related to the macro deformation regime and the overall mechanical response of the re-entrant honeycomb structure. Through the identification of elements undergoing the plastic strain of more than 10%, micro modes were successfully identified [216]. Incline loading on re-entrant honeycomb systems has also been studied in work by Dhari et al. [217]. Furthermore, a 3D re-entrant structure was also analysed under dynamic crushing conditions to observe its behaviour under extreme deformation [218].

Auxetic materials are also associated with impact resistance and have been proposed in applications of protective gear and automotive bumpers. Over the recent years, FEA has seen extensive use in exploring how auxetic materials behave in impact scenarios, significantly aiding material testing across industries such as automotive and aerospace industries. FEA offers a repeatable, non-destructive and rapid test, in lieu or in conjunction with the more time-consuming experimental tests. FEA protocols commonly investigate how auxetic materials respond to impact by analysing the dispersal and redirection of the force, as well as the energy absorption properties. This has proven particularly useful in analysing the crushing patterns and the deformations. For instance, Liu et al. showcased the behaviour of re-entrant auxetic honeycombs under different loading speeds [219]. Meanwhile, Guo et al. examined the impact of velocity and indenter size on a double U honeycomb structure (Figure 2f), and found it to exhibit superior energy absorption capacity and stress distribution compared to the conventional counterpart [143]. Similar to the work above, FEA has been instrumental in assessing the impact velocity and crashworthiness of auxetic structures, including a number of honeycombs [220] and modified honeycombs [144], hierarchical honeycombs [211] and chiral auxetic structures [152].
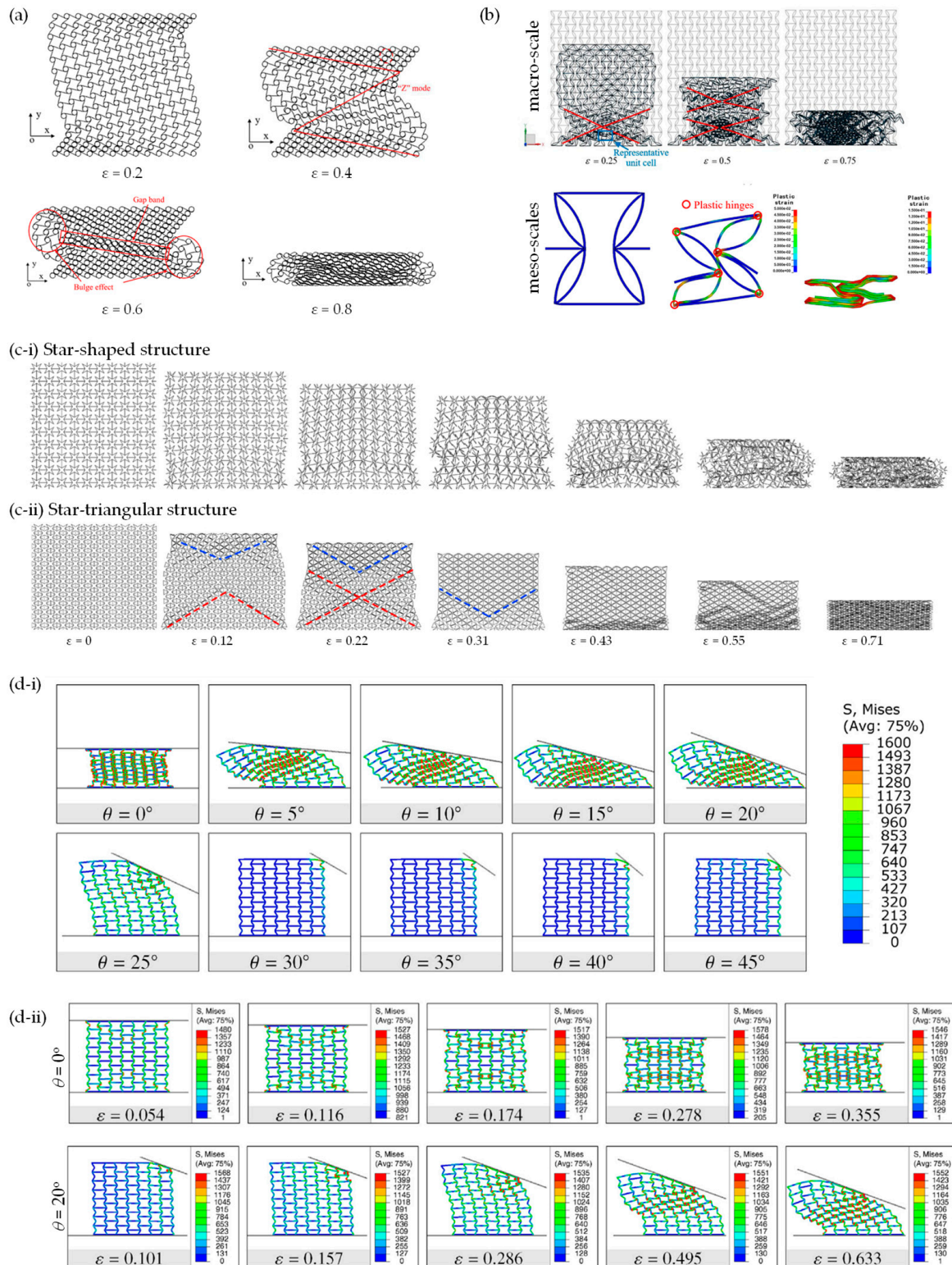
Figure 8. The crushing of auxetics as simulated by FEA: (**a**) quasi-static crushing at different extents of the global strains of tetrachiral honeycomb as summated by Qi et al. [154] at a velocity of 1 m/s; (**b**) predicted deformation processes of a re-entrant circular auxetic honeycombs specimen at typical states in the macro- and mesoscale as simulated by Qi et al. [214]; (**c**) the crushing of "star" honeycombs as simulated by Wei et al. [215]; (**d**) static inclined compression of re-entrant honeycomb auxetic structure as simulated by Singh et al. [216], where (**d-i**) shows the effect of angle of the inclination θ of how the load is applied and (**d-ii**) focuses on the system where $\theta = 0°$, $20°$, showing the deformation at different extents of applied strain.

A number of studies have used FEA to investigate the effect of indentation on the deformation mechanism [17]. In recent studies, FEA served to validate findings on the indentation resistance of the hexagonal honeycombs [221] and the indentation behaviour of 3D-printed auxetic reinforced composites [222]. Moreover, a recent study by Attard et al. looked at indentation from the perspective of the indenter. FEA was employed to examine the response of a finger-like indenter made from an inner hardcore (representing bone) surrounded by a softer outer layer (representing flesh) when pressing on a hard sample lined with an auxetic or conventional softer materials. This study revealed that although the auxetic material, with a highly negative Poisson's ratio, may feel harder when compared to a conventional material of the same Young's modulus, the auxetic does not have the "bottoming up" disadvantage and, thus, a thinner layer of auxetic can replace a much thicker conventional protective layer. Another emerging direction of studies [223] is the examination of the dynamic properties of auxetics. This is due to a multitude of potential applications that include acoustic absorbers [224–227], seismic insulators [228–231], energy harvesting devices [232,233] and artificial intelligence [234,235]. To assess the dynamic properties of the system through the FEM simulations, the first step typically corresponds to the determination of its phononic band structure. A common approach in this case is the use of a single unit cell with Floquet periodic boundary conditions. The resulting phononic band structure provides a plethora of information about the properties of the system ranging from the group and phase velocities of waves propagating through the system [236] to the phononic band gaps [237–239], as well as other more complex topological effects [240–242]. The possibility of finding the phononic band gaps is of practical importance since it allows the determination of ranges of frequencies at which waves are not transmitted through the system. The Bragg band gaps [243] can be observed once the effective wavelength of the wave propagating through the structure is approximately twice as large as the lattice constant of a metamaterial acting as a phononic crystal [244–246]. Over the years, a multitude of studies have been conducted on this topic to identify different classes of metamaterials that could act as wave insulators at various ranges of frequencies. These studies have been reported for devices at very different size scales [247] that corresponded to considerable band gaps at a broad range of frequencies including megahertz [248], kilohertz [249–252] as well as even lower frequencies related, for example, to seismic applications [228,253,254].

An important aspect that merges the worlds of static and dynamic properties of metamaterials is the possibility of controlling the phononic band structure through structural reconfiguration. In the case of a majority of metamaterials, to significantly modify the phononic band structure and the corresponding band gaps. it is necessary to change the system either by modifying the dimensions of its structural components [255] or by artificially changing the mass of the system, for example, by adding elements having a nonzero mass [256,257]. Despite the effectiveness of these approaches, these methods share the limitation that it is impossible to change the behaviour of the system without fabricating it again. There are also literature examples of metamaterials where the quasi-static mechanical reconfiguration influences the system to the point that its vibration modes change compared to the initial structure. For such scenarios, the entire band structure can indeed be considerably modified. It should be noted that this goal, to a moderate extent, can be achieved even for relatively simple geometries that are often studied from the perspective of their static properties [258–261]. Nonetheless, a greater change in the band structure can typically be observed for more complex or multistable systems that can be controlled even via external stimuli [262–264].

In conclusion, the studies reviewed here demonstrate the usefulness of FEA in analysing the mechanical properties and energy absorption capacity of these materials. FEA was pivotal in illustrating the great potential that auxetics have for applications requiring high-energy absorption capacity, such as in the automotive and aerospace industries.

4. Design of Products

FEA excels at replicating testing scenarios and analysing the behaviour of material within a specific scenario. Its application is not limited to replicating what is typically measured in conventional lab testing; rather, it can be extended to replicate the conditions in which the product is expected to perform, enabling the observation of its response.

Chow et al. proposed the use of 3D-printed thermoplastic polyurethane (TPU) with an auxetic architecture insert for pressure therapy to treat hypertrophic scars. The auxetic structure was designed to easily accommodate the contours of the human body during joint movements. The concept was initially tested in FEA examining the synclastic effect of out-of-plane bending. Subsequently, the formability, structural deformation and auxetic response of re-entrant and double arrowhead auxetic structures were numerically evaluated, followed by an experimental prototype. The study successfully demonstrated how the design was able to facilitate a stable level of pressure during body motion, promoting the recovery of hypertrophic scars [265].

In the construction industry, Menon et al. used FEA to observe the deflection behaviour of basic auxetic re-entrant beams and proposed an improvement to auxetic beam designs, comparing them with traditional beams when used in constructing a lightweight bridge (Figure 9a). The FEA analysis showed that the new auxetic beam designs exhibited better properties with minimal deflection, enhanced load-bearing capacity and a 64% reduction in material [266]. Another study [267] also used FEA to investigate auxetic honeycomb sandwich panels for structural applications. These panels offered reduced weight and displayed a remarkable reduction in the radiated sound power level due to the sandwich structure with an auxetic core [267]. It is important to note that FEA simulations of auxetics extend beyond mechanical scenarios such as uniaxial loading, shearing, pressing, crushing or indenting to encompass more complex scenarios essential for advanced applications. In particular, FEA was extensively used in acoustic and vibration frequency analysis of auxetics. For instance, in two studies by Li et al., the authors developed and applied a FEM to evaluate the propagation of acoustic and elastic waves through 3D phononic crystals. The method accurately computed band structures and identified band gaps and eigenmodes. The results showed that the finite element method was precise and efficient for computing band structures of complex phononic crystal structures with irregular unit shapes and could provide accurate results with commercial finite element code [268,269]. The research has been subsequently used by numerous studies [270,271] for numerical and experimental investigations of phononic crystal structures and the design of novel acoustic devices.

In a study by Li et al., fundamental frequencies were modelled for a structure comprising sandwich plates with a functionally graded (FG) auxetic 3D lattice core. Non-linear FEA revealed that the effects of FG configurations and strut incline angles are significant, with the FG-X specimen exhibiting the highest fundamental frequency. The study also investigated the large amplitude vibration characteristics of sandwich plates with an auxetic FG 3D lattice core in different thermal environments. Using full-scale non-linear FEA simulations, the effects of FG configurations on the natural frequencies, non-linear-to-linear frequency ratios of sandwich plates, and EPR amplitude curves were studied. Results indicate that the FG configurations distinctly affect the linear and non-linear vibration behaviour of sandwich plates, with EPR-amplitude curves stabilising when the vibration amplitude is sufficiently large. Overall, the study sheds light on the vibration behaviour of functionally graded auxetic 3D lattice metamaterials and sandwich plates with such core, offering insights for further investigations [272].

FEA has been applied in several studies to replicate the loading conditions of passenger vehicles to investigate different structures of auxetic non-pneumatic tyres [273–275] (Figure 9b). Additionally, it played a role in the design of anti-tetrachiral stents and hierarchical anti-tetrachiral stents with circular and elliptical nodes. Through FEA, the effects of stent geometrical parameters on the tensile mechanical behaviour of these stents were studied [62], as discussed previously.

Given the excellent ability of FEA to mimic high impacts, with adjustable impact velocities, indents and more, FEM has also been used to facilitate and explore the use of auxetics in military and sports equipment. FEA has already been used to predict material and product behaviour under certain conditions and to analyse design parameters in snowboard wrist protectors [276], helmets [41,277,278] and other sports equipment [279–281]. Mosleh et al. [278] used FEA to compare three scenarios involving helmets and head impact, namely an oblique head impact on foam at an angle of 45°, a linear impact of the helmeted head at an angle of 0° and a 45° oblique impact of the helmeted head (Figure 9c). In 2020, Airoldi et al. [282] studied foam-filled energy absorbers with auxetic behaviour for localized impacts and compared the results of FEA simulation to experimental results. A more recent study by Chen et al. (2023) employed FEA to investigate the effect of re-entrant arrowhead liners on helmet protection performance [283]. Through this study, it was illustrated that the auxetic lattice liners offer resistance to indentation, thereby enhancing the protection performance of the helmet [283].

When developing PPE, it is also crucially important to consider how materials behave when bent. Auxetic materials possess the remarkable ability to adopt a dome-shaped curvature under bending, making them particularly desirable for integration into PPE. Research conducted by Easey et al. employed FEA to explore the dome shape configurations exhibited by various cellular geometries, including re-entrant, arrowhead, tri-chiral and hexagonal patterns [284]. Their study highlighted that auxetic cellular domes demonstrate lower indentation resistance under compressive loading compared to solid counterparts, underscoring their potential suitability for PPE applications [284].

Another property sought after in the development of PPE is energy absorption and crashworthiness. Auxetic materials demonstrate enhanced energy absorption and crashworthiness due to their distinctive negative Poisson's ratio, resulting in compression-induced compaction. This property is also sought after in the automotive and aircraft industries. In a recent study by Tan et al., FEA was employed to study the energy absorption and crushing performance of hierarchical honeycombs [285]. It was illustrated that the electric vehicle crashworthiness is remarkably improved by the application of the auxetic hierarchical crash box [285].

Within this context, FEA has been employed to investigate the effects of unit-cell geometry and Poisson's ratio on mechanical properties in auxetic structures and plates. Additionally, FEA has been utilised to analyse the potential of auxetic constituents in composite materials, as demonstrated in the comparison between FEA and experimental analysis (Figure 9d) [286,287].

Several studies have investigated the ballistic impact behaviour of auxetic materials. In a study by Novak, chiral auxetic cellular structures were tested to analyse the effect of ballistic velocity and the deformation behaviour of composite sandwich panels. The experimental results validated the computational model of cover plates, which was further utilised to develop computational models of auxetic composite sandwich panels. The study shows that by using the auxetic sandwich panel, the ballistic performance is enhanced compared to monolithic cover plates [288,289]. In a recent study, the ballistic impact behaviour of auxetic sandwich composite human body armour was analysed using FEA. Numerical simulations showed improved indentation resistance and higher energy absorption in the auxetic armour compared to conventional monolithic armour [61]. Similar auxetic sandwich panels were also considered for blast protection in military vehicles, showcasing superior performance both in terms of being more lightweight and offering better protection compared to the solid plate [290]. Additionally, other studies also investigated the use of auxetics in body protection pads [291].
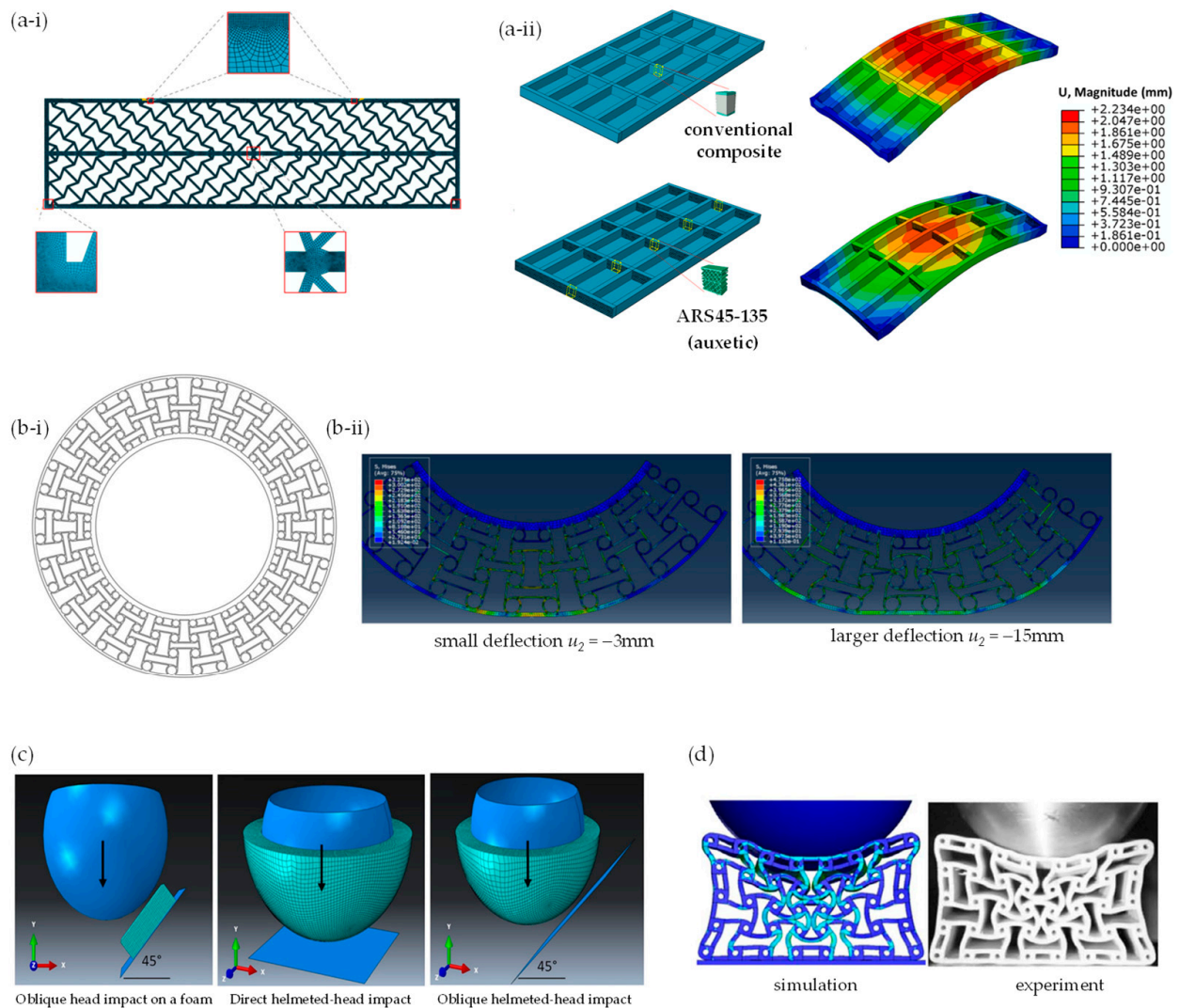
Figure 9. FEA of auxetics and product design: (**a**) auxetic beams for use in the construction industry by Menon et al. (2022) [266], where (**a-i**) shows the ARS45-135 auxetic beam and (**a-ii**) compares this beam to a conventional sandwich-panel beam in lightweight bridge construction; (**b**) non-pneumatic tyres investigated by Wu et al. (2022) [274], where (**b-i**) shows the profile in 2D and (**b-ii**) shows the results of FEA-simulated deformations; (**c**) helmet design as studied by Mosleh et al. (2018) [278] who examined direct and oblique head/helmet impacts; and (**d**) a comparison of FEA with simulated impact for application in sports equipment as reported by Shepherd et al., 2020.

5. Conclusions, Additional Considerations and Future Directions

This work demonstrated how FEA gradually became an essential tool in developing and understanding the mechanical properties of 2D and 3D auxetic cellular solids, such as honeycomb structures, as well as other auxetic materials, metamaterials and structures. This was only possible through advances in computational sciences. More specifically, FEA is particularly valuable in understanding auxetic behaviour, enabling the precise identification of stresses and strains within materials and metamaterials when loaded, which may not be easily demonstrated through experiments [292]. It is also especially beneficial to simulate characteristics which can only be tested using expensive equipment.

With time, FEA was used to simulate more real and complex scenarios required for end-product design. Some key studies attempted to optimise the geometry of auxetics to elicit superior properties. Thus, FEA was used to optimise the shape of novel auxetic structures and to determine their mechanical properties prior to prototyping and experimental testing.

Since the early years of auxetics, FEA emerged as a fundamental research tool for quick and reliable analysis during the design stage, reducing the need for physical prototyping, thereby accelerating advances in the field. Further advances are still needed, particularly in niche scenarios such as the exploration of new material compositions, granular materials [293], or hybrid auxetic structures combining different mechanisms of auxeticity. Such investigations could further optimize the existing properties of auxetic materials and even uncover new potential applications. Moreover, while FEA provides valuable insights into the mechanical behaviour of auxetic materials, it would be beneficial to extend the analysis to more specific and realistic application scenarios. This includes exploring variable environmental conditions, such as temperature or pressure variations, as well as exposure to UV, moisture, chemicals, biological species (e.g., mould), etc. to assess the reliability and durability of auxetic materials under real operational conditions.

Like any other experimental or simulation method, FEA has its strengths and limitations, and properly appreciating these limitations ensures that any results obtained are not artefacts of the simulation. One of its limitations is its relative complexity. When considering model building and inputting, the accuracy of the simulation results depend on how the system is entered into the FEA package. Structures are modelled as a continuum and, therefore, it is not possible to accurately model molecular systems. Even for substructures which can be treated as a continuum (for example, in metamaterials and high resolution additively manufactured cellular structures), the structures can still be so small that the number of elements and processing capacities outstrip "normal" computing capabilities. Furthermore, to further validate the results of FEA simulations, it is recommended to integrate the work with a greater amount of experimental data. This could involve advanced mechanical testing to verify the response of auxetic materials under various loads and in different environmental conditions. Integrating experimental data could help to better calibrate FEA simulations and increase their accuracy. The validation of such FEM solutions requires good sets of experimental data, but in this area, modelling and simulation are ahead of the experimental base, and experiments might not always be possible/feasible. This is particularly the case where non-linear, non-elastic, time-dependent and other dynamic phenomena (for example, snap-through processes in folded structures) are being modelled. Some other examples of complex systems which may be trivial to represent within an FEA environment include highly parametrised models, which study the effect of geometric parameters on properties (as is normally the case with modelling of auxetics); disordered systems such as cellular foams (auxetic and non-auxetic), where a representative unit does not exist and assumptions/simplifications need to be made; molecular-level systems where, as discussed elsewhere [197], scalability issues become prominent as the molecular-level interactions cannot be adequately represented through a mechanical model; and realistic systems having some degree of imperfections due to the manufacturing process. To address some of these limitations, it is necessary to construct more complex models than what is currently in the literature, something which will increase the computational cost of the simulations.

Another limitation of FEA is that the quality of the simulations typically relies on the properties of the intrinsic materials. In some cases, these are not easy to define and the material properties are unmeasured (as is the case with the simulations of systems made from hypothetical auxetic materials, e.g., [13,93]) or are entered in an over simplified way, such as by assuming that the material is behaving linearly, thereby mitigating against high computational costs. Such assumptions may reduce the applicability and accuracy of the simulated characteristics, which calls for further validation.

Two critical aspects in FEA are the boundary conditions applied (which in the case of the modelling of auxetics, includes situations where one needs to apply full periodic boundary conditions) and the manner in which loads/deformations are applied (uniaxial stretching of auxetics is typically simulated by applying a fixed displacement on a boundary to mimic the application of uniaxial strain, or by applying a force to mimic the application of stress). Moreover, successful finite element simulation requires many key factors to be taken

into consideration such as mesh size, mesh type and the constitutive relationship of the matrix material. To ensure that these key aspects of the methodology are correctly applied, it is essential to validate the protocol used, for example, by carrying out convergence testing to ensure that the meshing is sufficiently fine, particularly in regions close to points of impact, joints, regions of high-stress concentration, etc., yet not excessively fine to avoid increasing computational requirements unnecessarily.

Future directions for the modelling of auxetic materials are likely to focus on several key areas. There is a great need to better integrate atomic length-scale modelling and microstructural modelling to bridge the gaps between the length scales and time scales. While commercial FEA packages offer sophisticated pre- and post-processing capabilities, molecular-level modelling remains challenging. There is also significant potential for improvement in the modelling of non-linear, non-elastic, large strain, time-dependent and other dynamic phenomena. A major challenge in this area is the lack of sufficiently large sets of experimental data to validate such models. Establishing a free-to-use central database could greatly facilitate progress in this regard. Current FEM also lacks significant "predictive" capabilities, particularly in the development of radically new architectures. It is anticipated that the integration of AI techniques combined with FEM approaches could offer promising avenues for progress in this area. Finally, the field of metamaterials is enabling the development of a much broader range of "anomalous" properties such as a negative Poisson's ratio, negative thermal expansion coefficients, negative stiffness, negative mass, etc. These novel metamaterials have the potential to transcend traditional thermodynamic constraints. They can interact both mechanically and electromagnetically and have the ability to draw on external energy sources to drive their anomalous behaviour. This lack of constraint effectively bypasses normal physical constraints at the "material" level (although not at the "system" level). FEM and related methods will need considerable development to cope with the complexities of these new scenarios.

On a final note, it is crucial to consider the environmental impact and sustainability in the design and the application of auxetic materials. This could involve conducting a life cycle analysis of auxetic materials, from production, to use, to disposal. Such analysis can promote the development of materials that are not only technologically advanced but also environmentally sustainable.

Appendix A

Table A1. Examples of works on auxetics classified according to the software used.

Program Used	2D/3D	References
ABAQUS	2D	[17,55,58,64,65,111,112,138–140,142,143,155,184,185,209,216,219,220,222,266,269]
	3D	[56,60,62,63,66,92,107,109,110,113,127–129,134,137,144–146,149,151,152,187,188,190–192,194,196,199,201,208,210,213,218,272,274,282,290,292]
ANSYS	2D	[94,95,97,135,150,157–159,161–166,172,174,182,212,221]
	3D	[57,61,96,105,108,131,136,141,160,167,171,177,183,193,267,273]
Other	2F	[59,130,170,173,176,186,211,214,215,270]
	3D	[18,132,133,153,154,189,202,207,265,268,275,276,288,289]

Table A2. Examples of works on auxetics classified according to the characteristic studied.

Property Studied	2D/3D	References
Auxeticity and stiffness	2D	[58,64,65,94,95,97,111,130,135,138–140,142,143,150,155,157–159,161–165,170,172–174,176,182,184,185,266]
	3D	[56,57,60,62,63,66,92,108,110,113,128,129,131,134,136,137,141,145,149,160,171,177,183,187,189–194,196,199,201,274,275,292]
Energy absorption and indentation, impact and blast resistance	2D	[17,112,209,211,212,214,215,219–222]
	3D	[18,57,61,63,92,107,109,127,132,133,144,151–154,188,194,202,204,205,207,208,210,213,218,273,276,282,288–290]
Other	2D	[166,269,270]
	3D	[265,267,268,272]

References

1. Evans, K.E.; Nkansah, M.A.; Hutcherson, I.J.; Rogers, S.C. Molecular Network Design. *Nature* **1991**, *353*, 124. [CrossRef]
2. Wojciechowski, K.W. Two-Dimensional Isotropic System with a Negative Poisson Ratio. *Phys. Lett. A* **1989**, *137*, 60–64. [CrossRef]
3. Lakes, R. Foam Structures with a Negative Poisson's Ratio. *Science* **1987**, *235*, 1038–1040. [CrossRef] [PubMed]
4. Lempriere, B.M. Poisson's Ratio in Orthotropic Materials. *Am. Inst. Aeronaut. Astronaut. J.* **1968**, *6*, 2226–2227. [CrossRef]
5. Wojciechowski, K.W. Remarks on "Poisson Ratio beyond the Limits of the Elasticity Theory". *J. Phys. Soc. Jpn.* **2003**, *72*, 1819–1820. [CrossRef]
6. Keskar, N.R.; Chelikowsky, J.R. Negative Poisson Ratios in Crystalline SiO_2 from First-Principles Calculations. *Nature* **1992**, *358*, 222–224. [CrossRef]
7. Baughman, R.H.; Shacklette, J.M.; Zakhidov, A.A.; Stafströ, S. Negative Poisson's Ratios as a Common Feature of Cubic Metals. *Nature* **1998**, *392*, 362–365. [CrossRef]
8. Brańka, A.C.; Heyes, D.M.; Wojciechowski, K.W. Auxeticity of Cubic Materials. *Phys. Status Solidi* **2009**, *246*, 2063–2071. [CrossRef]
9. Brańka, A.C.; Heyes, D.M.; Wojciechowski, K.W. Auxeticity of Cubic Materials under Pressure. *Phys. Status Solidi* **2011**, *248*, 96–104. [CrossRef]
10. Goldstein, R.V.; Gorodtsov, V.A.; Lisovenko, D.S. Classification of Cubic Auxetics. *Phys. Status Solidi Basic Res.* **2013**, *250*, 2038–2043. [CrossRef]
11. Alderson, A. A Triumph of Lateral Thought. *Chem. Ind.* **1999**, *10*, 384–391.
12. Argatov, I.I.; Guinovart-Díaz, R.; Sabina, F.J. On Local Indentation and Impact Compliance of Isotropic Auxetic Materials from the Continuum Mechanics Viewpoint. *Int. J. Eng. Sci.* **2012**, *54*, 42–57. [CrossRef]
13. Attard, D.; Gatt, R.; Caruana-Gauci, R.; Grima-Cornish, J.N.; Cauchi, R.; Sillato, D.; Cerasola, D.; Ficarra, G.; Bezzina, D.S.; Formosa, C.; et al. What It could Feel like to Press on an Auxetic: Effect of Poisson's Ratio on the Indenter. *Smart Mater. Struct.* **2023**, *32*, 095038. [CrossRef]
14. Chan, N.; Evans, K.E. Indentation Resilience of Conventional and Auxetic Foams. *J. Cell. Plast.* **1998**, *34*, 231–260. [CrossRef]
15. Imbalzano, G.; Tran, P.; Ngo, T.D.; Lee, P.V.S. Three-Dimensional Modelling of Auxetic Sandwich Panels for Localised Impact Resistance. *J. Sandw. Struct. Mater.* **2015**, *19*, 291–316. [CrossRef]
16. Lakes, R.S.; Elms, K. Indentability of Conventional and Negative Poisson's Ratio Foams. *J. Compos. Mater.* **1993**, *27*, 1193–1202. [CrossRef]

17. Li, Z.; Wang, K.F.; Wang, B.L. Indentation Resistance of Brittle Auxetic Structures: Combining Discrete Representation and Continuum Model. *Eng. Fract. Mech.* **2021**, *252*, 107824. [CrossRef]

18. Novak, N.; Krstulović-Opara, L.; Ren, Z.; Vesenjak, M. Compression and Shear Behaviour of Graded Chiral Auxetic Structures. *Mech. Mater.* **2020**, *148*, 103524. [CrossRef]

19. Photiou, D.; Prastiti, N.; Sarris, E.; Constantinides, G. On the Conical Indentation Response of Elastic Auxetic Materials: Effects of Poisson's Ratio, Contact Friction and Cone Angle. *Int. J. Solids Struct.* **2016**, *81*, 33–42. [CrossRef]

20. Yang, S.; Chalivendra, V.B.; Kim, Y.K. Fracture and Impact Characterization of Novel Auxetic Kevlar®/Epoxy Laminated Composites. *Compos. Struct.* **2017**, *168*, 120–129. [CrossRef]

21. Alderson, K.L.; Simkins, V.R.; Coenen, V.L.; Davies, P.J.; Alderson, A.; Evans, K.E. How to Make Auxetic Fibre Reinforced Composites. *Phys. Status Solidi* **2005**, *242*, 509–518. [CrossRef]

22. Choi, J.B. Fracture Toughness of Re-Entrant Foam Materials with a Negative Poisson's Ratio: Experiment and Analysis. *Int. J. Fract.* **1996**, *80*, 73–83. [CrossRef]

23. Zouaoui, M.; Saifouni, O.; Gardan, J.; Makke, A.; Recho, N.; Kauffmann, J. Improvement of Fracture Toughness Based on Auxetic Patterns Fabricated by Metallic Extrusion in 3D Printing. *Procedia Struct. Integr.* **2022**, *42*, 680–686. [CrossRef]

24. Choi, J.B.; Lakes, R.S. Non-Linear Properties of Metallic Cellular Materials with a Negative Poisson's Ratio. *J. Mater. Sci.* **1992**, *27*, 5375–5381. [CrossRef]

25. Novak, N.; Duncan, O.; Allen, T.; Alderson, A.; Vesenjak, M.; Ren, Z. Shear Modulus of Conventional and Auxetic Open-Cell Foam. *Mech. Mater.* **2021**, *157*, 103818. [CrossRef]

26. Alomarah, A.; Yuan, Y.; Ruan, D. A Bio-Inspired Auxetic Metamaterial with Two Plateau Regimes: Compressive Properties and Energy Absorption. *Thin-Walled Struct.* **2023**, *192*, 111175. [CrossRef]

27. Zhang, X.G.; Jiang, W.; Zhang, Y.; Luo, C.; Zhang, X.Y.; Han, D.; Hao, J.; Teng, X.C.; Xie, Y.M.; Ren, X. Energy Absorption Properties of Composite Tubes with Hexagonal and Re-Entrant Honeycomb Fillers. *Constr. Build. Mater.* **2022**, *356*, 129298. [CrossRef]

28. Asad, M.; Dhanasekar, M.; Zahra, T.; Thambiratnam, D. Impact Mitigation of Masonry Walls with Carbon Fibre and Auxetic Fibre Composite Renders—A Numerical Study. *Structures* **2020**, *28*, 2733–2751. [CrossRef]

29. Tao, Z.; Ren, X.; Zhao, A.G.; Sun, L.; Zhang, Y.; Jiang, W.; Han, D.; Zhang, X.Y.; Xie, Y.M. A Novel Auxetic Acoustic Metamaterial Plate with Tunable Bandgap. *Int. J. Mech. Sci.* **2022**, *226*, 107414. [CrossRef]

30. Xu, Y.; Schlangen, E.; Luković, M.; Šavija, B. Tunable Mechanical Behavior of Auxetic Cementitious Cellular Composites (CCCs): Experiments and Simulations. *Constr. Build. Mater.* **2021**, *266*, 121388. [CrossRef]

31. Zhang, Q.; Sun, Y. A Series of Auxetic Metamaterials with Negative Thermal Expansion Based on L-Shaped Microstructures. *Thin-Walled Struct.* **2024**, *197*, 111596. [CrossRef]

32. Arjunan, A.; Zahid, S.; Baroutaji, A.; Robinson, J. 3D Printed Auxetic Nasopharyngeal Swabs for COVID-19 Sample Collection. *J. Mech. Behav. Biomed. Mater.* **2021**, *114*, 104175. [CrossRef] [PubMed]

33. Liu, J.; Yao, X.; Wang, Z.; Ye, J.; Luan, C.; He, Y.; Lin, H.; Fu, J. A Flexible Porous Chiral Auxetic Tracheal Stent with Ciliated Epithelium. *Acta Biomater.* **2021**, *124*, 153–165. [CrossRef] [PubMed]

34. Scarpa, F. Auxetic Materials for Bioprostheses. *IEEE Signal Process. Mag.* **2008**, *25*, 126–128. [CrossRef]

35. Song, L.; Ahmed, M.F.; Li, Y.; Zeng, C.; Li, Y. Vascular Differentiation from Pluripotent Stem Cells in 3-D Auxetic Scaffolds. *J. Tissue Eng. Regen. Med.* **2018**, *12*, 1679–1689. [CrossRef]

36. Yan, Y.; Li, Y.; Song, L.; Zeng, C.; Li, Y. Pluripotent Stem Cell Expansion and Neural Differentiation in 3-D Scaffolds of Tunable Poisson's Ratio. *Acta Biomater.* **2017**, *49*, 192–203. [CrossRef] [PubMed]

37. Yao, Y.; Yuan, H.; Huang, H.; Liu, J.; Wang, L.; Fan, Y. Biomechanical Design and Analysis of Auxetic Pedicle Screw to Resist Loosening. *Comput. Biol. Med.* **2021**, *133*, 104386. [CrossRef]

38. Allen, T.; Martinello, N.; Zampieri, D.; Hewage, T.; Senior, T.; Foster, L.; Alderson, A. Auxetic Foams for Sport Safety Applications. *Procedia Eng.* **2015**, *112*, 104–109. [CrossRef]

39. Cross, T.M.; Hoffer, K.W.; Jones, D.P.; Kirschner, P.B.; Langvin, E.; Meschter, J.C. Auxetic Structures and Footwear with Soles Having Auxetic Structures. U.S. Patent Application No. 9402439B2, 2 August 2016.

40. Duncan, O.; Bailly, N.; Allen, T.; Petit, Y.; Wagnac, E.; Alderson, A. Effect of Compressive Strain Rate on Auxetic Foam. *Appl. Sci.* **2021**, *11*, 1207. [CrossRef]

41. Foster, L.; Peketi, P.; Allen, T.; Senior, T.; Duncan, O.; Alderson, A. Application of Auxetic Foam in Sports Helmets. *Appl. Sci.* **2018**, *8*, 354. [CrossRef]

42. Hanna, B.; Adams, R.; Townsend, S.; Robinson, M.; Soe, S.; Stewart, M.; Burek, R.; Theobald, P. Auxetic Metamaterial Optimisation for Head Impact Mitigation in American Football. *Int. J. Impact Eng.* **2021**, *157*, 103991. [CrossRef]

43. Hassanin, H.; Abena, A.; Elsayed, M.A.; Essa, K. 4D Printing of NiTi Auxetic Structure with Improved Ballistic Performance. *Micromachines* **2020**, *11*, 745. [CrossRef] [PubMed]

44. Jacobs, M.J.N.; Van Dingenen, J.L.J. Ballistic Protection Mechanisms in Personal Armour. *J. Mater. Sci.* **2001**, *36*, 3137–3142. [CrossRef]

45. Steffens, F.; Oliveira, F.R.; Fangueiro, R. Energy Absorption from Composite Reinforced with High Performance Auxetic Textile Structure. *J. Compos. Mater.* **2021**, *55*, 1003–1013. [CrossRef]

46. Underhill, R. Defense Applications of Auxetic Materials. *Def. Syst. Inf. Anal. Cent. J.* **2014**, *1*, 7–13.

47. Minetola, P.; Giubilini, A. Multimaterial 3D Printing of Auxetic Jounce Bumpers for Automotive Suspensions. *Rapid Prototyp. J.* **2023**, *29*, 131–142. [CrossRef]

48. Wang, C.; Wang, W.; Zhao, W.; Wang, Y.; Zhou, G. Structure Design and Multi-Objective Optimization of a Novel NPR Bumper System. *Compos. Part B Eng.* **2018**, *153*, 78–96. [CrossRef]

49. Zhao, Y.; Zhang, Q.; Li, Y.; Wang, B.; Ma, F. Theoretical, Emulation and Experimental Analysis on Auxetic Re-Entrant Octagonal Honeycombs and Its Applications on Pedestrian Protection of Engine Hood. *Compos. Struct.* **2021**, *260*, 113534. [CrossRef]

50. Lantada, A.D.; de Blas Romero, A.; Schwentenwein, M.; Jellinek, C.; Homa, J. Lithography-Based Ceramic Manufacture (LCM) of Auxetic Structures: Present Capabilities and Challenges. *Smart Mater. Struct.* **2016**, *25*, 54015. [CrossRef]

51. Lira, C.; Scarpa, F.; Rajasekaran, R. A Gradient Cellular Core for Aeroengine Fan Blades Based on Auxetic Configurations. *J. Intell. Mater. Syst. Struct.* **2011**, *22*, 907–917. [CrossRef]

52. Wang, Z.; Zulifqar, A.; Hu, H. Auxetic Composites in Aerospace Engineering. In *Advanced Composite Materials for Aerospace Engineering*; Elsevier: Amsterdam, The Netherlands, 2016; pp. 213–240.

53. Kim, Y.; Son, K.; Lee, J. Auxetic Structures for Tissue Engineering Scaffolds and Biomedical Devices. *Materials* **2021**, *14*, 6821. [CrossRef] [PubMed]

54. Shukla, S.; Behera, B.K. Auxetic Fibrous Materials and Structures in Medical Engineering—A Review. *J. Text. Inst.* **2022**, *114*, 1078–1089. [CrossRef]

55. Abbaslou, M.; Hashemi, R.; Etemadi, E. Novel Hybrid 3D-Printed Auxetic Vascular Stent Based on Re-Entrant and Meta-Trichiral Unit Cells: Finite Element Simulation with Experimental Verifications. *Mater. Today Commun.* **2023**, *35*, 105742. [CrossRef]

56. Ali, M.N.; Busfield, J.J.C.C.; Rehman, I.U. Auxetic Oesophageal Stents: Structure and Mechanical Properties. *J. Mater. Sci. Mater. Med.* **2014**, *25*, 527–553. [CrossRef] [PubMed]

57. Alomarah, A.; Ruan, D.; Masood, S.; Gao, Z. Compressive Properties of a Novel Additively Manufactured 3D Auxetic Structure. *Smart Mater. Struct.* **2019**, *28*, 085019. [CrossRef]

58. Alomarah, A.; Xu, S.; Masood, S.H.; Ruan, D. Dynamic Performance of Auxetic Structures: Experiments and Simulation. *Smart Mater. Struct.* **2020**, *29*, 055031. [CrossRef]

59. Khan, S.Z.; Mustahsan, F.; Mahmoud, E.R.I.; Masood, S.H. A Novel Modified Re-Entrant Honeycomb Structure to Enhance the Auxetic Behavior: Analytical and Numerical Study by FEA. *Mater. Today Proc.* **2019**, *39*, 1041–1045. [CrossRef]

60. Li, C.; Shen, H.S.; Wang, H. Full-Scale Finite Element Modeling and Nonlinear Bending Analysis of Sandwich Plates with Functionally Graded Auxetic 3D Lattice Core. *J. Sandw. Struct. Mater.* **2021**, *23*, 3113–3138. [CrossRef]

61. Shah, I.A.; Khan, R.; Koloor, S.S.R.; Petrů, M.; Badshah, S.; Ahmad, S.; Amjad, M. Finite Element Analysis of the Ballistic Impact on Auxetic Sandwich Composite Human Body Armor. *Materials* **2022**, *15*, 2064. [CrossRef]

62. Wu, W.; Song, X.; Liang, J.; Xia, R.; Qian, G.; Fang, D. Mechanical Properties of Anti-Tetrachiral Auxetic Stents. *Compos. Struct.* **2018**, *185*, 381–392. [CrossRef]

63. Yang, W.; Huang, R.; Liu, J.J.; Liu, J.J.; Huang, W. Ballistic Impact Responses and Failure Mechanism of Composite Double-Arrow Auxetic Structure. *Thin-Walled Struct.* **2022**, *174*, 109087. [CrossRef]

64. Zhang, J.; Lu, G.; Ruan, D.; Wang, Z. Tensile Behavior of an Auxetic Structure: Analytical Modeling and Finite Element Analysis. *Int. J. Mech. Sci.* **2018**, *136*, 143–154. [CrossRef]

65. Zhang, J.; Lu, G.; Wang, Z.; Ruan, D.; Alomarah, A.; Durandet, Y. Large Deformation of an Auxetic Structure in Tension: Experiments and Finite Element Analysis. *Compos. Struct.* **2018**, *184*, 92–101. [CrossRef]

66. Crespo, J.; Duncan, O.; Alderson, A.; Montáns, F.J. Auxetic Orthotropic Materials: Numerical Determination of a Phenomenological Spline-Based Stored Density Energy and Its Implementation for Finite Element Analysis. *Comput. Methods Appl. Mech. Eng.* **2020**, *371*, 113300. [CrossRef]

67. Wojciechowski, K.W. Constant Thermodynamic Tension Monte Carlo Studies of Elastic Properties of a Two-Dimensional System of Hard Cyclic Hexamers. *Mol. Phys.* **1987**, *61*, 1247–1258. [CrossRef]

68. Strek, T.; Maruszewski, B.T.B.; Narojczyk, J.W.; Wojciechowski, K.W. Finite Element Analysis of Auxetic Plate Deformation. *J. Non-Cryst. Solids* **2008**, *354*, 4475–4480. [CrossRef]

69. Narojczyk, J.W.; Alderson, A.; Imre, A.R.; Scarpa, F.; Wojciechowski, K.W. Negative Poisson's Ratio Behavior in the Planar Model of Asymmetric Trimers at Zero Temperature. *J. Non-Cryst. Solids* **2008**, *354*, 4242–4248. [CrossRef]

70. Madenci, E.; Guven, I. *The Finite Element Method and Applications in Engineering Using ANSYS®*, 2nd ed.; Springer: New York, NY, USA, 2015; ISBN 9781489975492.

71. Huebner, K.H.; Dewhirst, D.L.; Smith, D.E.; Byrom, T.G. *The Finite Element Method for Engineers*, 4th ed.; Wiley-Interscience: New York, NY, USA, 2001; ISBN 978-0471370789.

72. Courant, R. Variational Methods for the Solution of Problems of Equilibrium and Vibrations. *Bull. Am. Math. Soc.* **1943**, *49*, 1–23. [CrossRef]

73. Hrennikoff, A. Solution of Problems of Elasticity by the Framework Method. *J. Appl. Mech.* **1941**, *8*, A169–A175. [CrossRef]

74. Trivedi, S. Finite Element Analysis: A Boon to Dentistry. *J. Oral Biol. Craniofacial Res.* **2014**, *4*, 200–203. [CrossRef]

75. Wood, I.; Jawad, Z.; Paisley, C.; Brunton, P. Non-Carious Cervical Tooth Surface Loss: A Literature Review. *J. Dent.* **2008**, *36*, 759–766. [CrossRef] [PubMed]

76. Aparna, J.; Maiti, S.; Jessy, P. Polyether Ether Ketone—As an Alternative Biomaterial for Metal Richmond Crown-3-Dimensional Finite Element Analysis. *J. Conserv. Dent.* **2021**, *24*, 553. [CrossRef]

77. Srirekha, A.; Bashetty, K. Infinite to Finite: An Overview of Finite Element Analysis. *Indian J. Dent. Res.* **2010**, *21*, 425. [CrossRef] [PubMed]

78. Tatarciuc, M.; Maftei, G.A.; Vitalariu, A.; Luchian, I.; Martu, I.; Diaconu-Popa, D. Inlay-Retained Dental Bridges—A Finite Element Analysis. *Appl. Sci.* **2021**, *11*, 3770. [CrossRef]

79. Thresher, R.W.; Saito, G.E. The Stress Analysis of Human Teeth. *J. Biomech.* **1973**, *6*, 443–449. [CrossRef] [PubMed]

80. Valera-Jiménez, J.F.; Burgueño-Barris, G.; Gómez-González, S.; López-López, J.; Valmaseda-Castellón, E.; Fernández-Aguado, E. Finite Element Analysis of Narrow Dental Implants. *Dent. Mater.* **2020**, *36*, 927–935. [CrossRef] [PubMed]

81. Galbusera, F.; Casaroli, G.; Chande, R.; Lindsey, D.; Villa, T.; Yerby, S.; Mesiwala, A.; Panico, M.; Gallazzi, E.; Brayda-Bruno, M. Biomechanics of Sacropelvic Fixation: A Comprehensive Finite Element Comparison of Three Techniques. *Eur. Spine J.* **2020**, *29*, 295–305. [CrossRef] [PubMed]

82. Huiskes, R.; Chao, E.Y.S. A Survey of Finite Element Analysis in Orthopedic Biomechanics: The First Decade. *J. Biomech.* **1983**, *16*, 385–409. [CrossRef]

83. Mengoni, M. Biomechanical Modelling of the Facet Joints: A Review of Methods and Validation Processes in Finite Element Analysis. *Biomech. Model. Mechanobiol.* **2020**, *20*, 389–401. [CrossRef]

84. Phellan, R.; Hachem, B.; Clin, J.; Mac-Thiong, J.M.; Duong, L. Real-Time Biomechanics Using the Finite Element Method and Machine Learning: Review and Perspective. *Med. Phys.* **2021**, *48*, 7–18. [CrossRef]

85. Cremonesi, M.; Franci, A.; Idelsohn, S.; Oñate, E. A State of the Art Review of the Particle Finite Element Method (PFEM). *Arch. Comput. Methods Eng.* **2020**, *27*, 1709–1735. [CrossRef]

86. Fadiji, T.; Coetzee, C.J.; Berry, T.M.; Ambaw, A.; Opara, U.L. The Efficacy of Finite Element Analysis (FEA) as a Design Tool for Food Packaging: A Review. *Biosyst. Eng.* **2018**, *174*, 20–40. [CrossRef]

87. Liang, X.; Ali, M.Z.; Zhang, H. Induction Motors Fault Diagnosis Using Finite Element Method: A Review. *IEEE Trans. Ind. Appl.* **2020**, *56*, 1205–1217. [CrossRef]

88. Müzel, S.D.; Bonhin, E.P.; Guimarães, N.M.; Guidi, E.S. Application of the Finite Element Method in the Analysis of Composite Materials: A Review. *Polymers* **2020**, *12*, 818. [CrossRef] [PubMed]

89. Gao, J.; Xu, W.; Ding, Z. 3D Finite Element Mesh Generation of Complicated Tooth Model Based on CT Slices. *Comput. Methods Programs Biomed.* **2006**, *82*, 97–105. [CrossRef] [PubMed]

90. Moens, D.; Vandepitte, D. Recent Advances in Non-Probabilistic Approaches for Non-Deterministic Dynamic Finite Element Analysis. *Arch. Comput. Methods Eng.* **2006**, *13*, 389–464. [CrossRef]

91. Viceconti, M.; Zannoni, C.; Testi, D.; Petrone, M.; Perticoni, S.; Quadrani, P.; Taddei, F.; Imboden, S.; Clapworthy, G. The Multimod Application Framework: A Rapid Application Development Tool for Computer Aided Medicine. *Comput. Methods Programs Biomed.* **2007**, *85*, 138–151. [CrossRef] [PubMed]

92. Wang, L.; Ulliac, G.; Wang, B.; Iglesias Martínez, J.A.; Dudek, K.K.; Laude, V.; Kadic, M. 3D Auxetic Metamaterials with Elastically-Stable Continuous Phase Transition. *Adv. Sci.* **2022**, *9*, 2204721. [CrossRef]

93. Attard, D.; Caruana-Gauci, R.; Cerasola, D.; Grima-Cornish, J.N.; Bezzina, D.S.; Ficarra, G.; Grima, J.N. On the Effect of the Poisson's Ratio on Samples Subjected to Shearing. *Eng. Res. Express* **2023**, *5*, 035044. [CrossRef]

94. Evans, K.E.; Nkansah, M.A.; Hutchinson, I.J. Modelling Negative Poisson Ratio Effects in Network-Embedded Composites. *Acta Metall. Mater.* **1992**, *40*, 2462–2469. [CrossRef]

95. Nkansah, M.A.; Evans, K.E.; Hutchinson, I.J. Modelling the Mechanical Properties of an Auxetic Molecular Network. *Model. Simul. Mater. Sci. Eng.* **1994**, *2*, 337–352. [CrossRef]

96. Evans, K.E.; Nkansah, M.A.; Hutchinson, I.J. Auxetic Foams: Modelling Negative Poisson's Ratios. *Acta Metall. Mater. mater.* **1994**, *42*, 1289–1294. [CrossRef]

97. Nkansah, M.A.; Evans, K.E.; Hutchinson, I.J. Modelling the Effects of Negative Poisson's Ratios in Continuous-Fibre Composites. *J. Mater. Sci.* **1993**, *28*, 2687–2692. [CrossRef]

98. Alderson, A.; Evans, K.E. Microstructural Modelling of Auxetic Microporous Polymers. *J. Mater. Sci.* **1995**, *30*, 3319–3332. [CrossRef]

99. Sigmund, O. *Design of Material Structures Using Topology Optimization*; Technical University of Denmark: Kongens Lyngby, Denmark, 1994.

100. Larsen, U.D.; Sigmund, O.; Bouwstra, S. Design and Fabrication of Compliant Micromechanisms and Structures with Negative Poisson's Ratio. *J. Microelectromech. Syst.* **1997**, *6*, 99–106. [CrossRef]

101. Sigmund, O.; Torquato, S. Design of Smart Composite Materials Using Topology Optimization. *Smart Mater. Struct.* **1999**, *8*, 365–379. [CrossRef]

102. Grima, J.N.; Gatt, R.; Farrugia, P.-S. On the Properties of Auxetic Meta-Tetrachiral Structures. *Phys. Status Solidi* **2008**, *245*, 511–520. [CrossRef]

103. Gatt, R.; Attard, D.; Farrugia, P.-S.; Azzopardi, K.M.; Mizzi, L.; Brincat, J.-P.; Grima, J.N. A Realistic Generic Model for Anti-Tetrachiral Systems. *Phys. Status Solidi* **2013**, *250*, 2012–2019. [CrossRef]

104. Alderson, A.; Alderson, K.L.; Attard, D.; Evans, K.E.; Gatt, R.; Grima, J.N.; Miller, W.; Ravirala, N.; Smith, C.W.; Zied, K. Elastic Constants of 3-, 4- and 6-Connected Chiral and Anti-Chiral Honeycombs Subject to Uniaxial in-Plane Loading. *Compos. Sci. Technol.* **2010**, *70*, 1042–1048. [CrossRef]

105. Afshar, A.; Rezvanpour, H. Computational Study of Non-Porous Auxetic Plates with Diamond Shape Inclusions. *J. Compos. Sci.* **2022**, *6*, 192. [CrossRef]
106. Chen, K.; Gao, Q.; Fang, S.; Zou, D.; Yang, Z.; Liao, W.H. An Auxetic Nonlinear Piezoelectric Energy Harvester for Enhancing Efficiency and Bandwidth. *Appl. Energy* **2021**, *298*, 117274. [CrossRef]
107. Gunaydin, K.; Turkmen, H.S. In-Plane Quasi-Static Crushing Finite Element Analysis of Auxetic Lattices. In Proceedings of the 2019 9th International Conference on Recent Advances in Space Technologies (RAST), Istanbul, Turkey, 11–14 June 2019; pp. 645–648. [CrossRef]
108. Kavakli, H.S.; Ali, D. Enhancing the Mechanical Properties of Auxetic Metamaterials by Incorporating Nonrectangular Cross Sections into Their Component Rods: A Finite Element Analysis. *Phys. Status Solidi* **2023**, *260*, 2200194. [CrossRef]
109. Logakannan, K.P.; Ramachandran, V.; Rengaswamy, J.; Ruan, D. Stiffened Star-Shaped Auxetic Structure with Tri-Directional Symmetry. *Compos. Struct.* **2022**, *279*, 114773. [CrossRef]
110. Rad, M.S.; Hatami, H.; Ahmad, Z.; Yasuri, A.K. Analytical Solution and Finite Element Approach to the Dense Re-Entrant Unit Cells of Auxetic Structures. *Acta Mech.* **2019**, *230*, 2171–2185. [CrossRef]
111. Wei, Y.L.; Yang, Q.S.; Tao, R. SMP-Based Chiral Auxetic Mechanical Metamaterial with Tunable Bandgap Function. *Int. J. Mech. Sci.* **2021**, *195*, 106267. [CrossRef]
112. Xu, W.; Dong, Z.; Ma, P. Finite Element Analyses of Auxetic Warp-Knitted Fabric Deformation Behaviors under Low-Velocity Impact Loading. *J. Text. Inst.* **2020**, *111*, 1578–1586. [CrossRef]
113. Zhang, X.Y.; Ren, X.; Wang, X.Y.; Zhang, Y.; Xie, Y.M. A Novel Combined Auxetic Tubular Structure with Enhanced Tunable Stiffness. *Compos. Part B Eng.* **2021**, *226*, 109303. [CrossRef]
114. Javanbakht, Z.; Öchsner, A. *Advanced Finite Element Simulation with MSC Marc*; Springer International Publishing: Cham, Switzerland, 2017; ISBN 9783319476674.
115. Borovinsek, M.; Novak, N.; Vesenjak, M.; Ren, Z.; Ulbin, M. Designing 2D Auxetic Structures Using Multi-Objective Topology Optimization. *Mater. Sci. Eng. A* **2020**, *795*, 139914. [CrossRef]
116. Almgren, R.F. An Isotropic Three-Dimensional Structure with Poisson's Ratio = −1. *J. Elast.* **1985**, *15*, 427–430. [CrossRef]
117. Gibson, L.J.J.; Ashby, M.F.F.; Schajer, G.S.S.; Robertson, C.I.I. The Mechanics of Two-Dimensional Cellular Materials. *Proc. R. Soc. A Math. Phys. Eng. Sci.* **1982**, *382*, 25–42. [CrossRef]
118. Grima, J.N.; Attard, D.; Ellul, B.; Gatt, R. An Improved Analytical Model for the Elastic Constants of Auxetic and Conventional Hexagonal Honeycombs. *Cell. Polym.* **2011**, *30*, 287–310. [CrossRef]
119. Sigmund, O. Tailoring Materials with Prescribed Elastic Properties. *Mech. Mater.* **1995**, *20*, 351–368. [CrossRef]
120. Sigmund, O. Materials with Prescribed Constitutive Parameters: An Inverse Homogenization Problem. *Int. J. Solids Struct.* **1994**, *31*, 2313–2329. [CrossRef]
121. Zhu, B.; Zhang, X.; Zhang, H.; Liang, J.; Zang, H.; Li, H.; Wang, R. Design of Compliant Mechanisms Using Continuum Topology Optimization: A Review. *Mech. Mach. Theory* **2020**, *143*, 103622. [CrossRef]
122. Zheng, Y.; Wang, Y.; Lu, X.; Liao, Z.; Qu, J. Evolutionary Topology Optimization for Mechanical Metamaterials with Auxetic Property. *Int. J. Mech. Sci.* **2020**, *179*, 105638. [CrossRef]
123. Schwerdtfeger, J.; Wein, F.; Leugering, G.; Singer, R.F.; Körner, C.; Stingl, M.; Schury, F. Design of Auxetic Structures via Mathematical Optimization. *Adv. Mater.* **2011**, *23*, 2650–2654. [CrossRef] [PubMed]
124. Clausen, A.; Wang, F.; Jensen, J.S.; Sigmund, O.; Lewis, J.A. Topology Optimized Architectures with Programmable Poisson's Ratio over Large Deformations. *Adv. Mater.* **2015**, *27*, 5523–5527. [CrossRef] [PubMed]
125. Bruggi, M.; Zega, V.; Corigliano, A. Synthesis of Auxetic Structures Using Optimization of Compliant Mechanisms and a Micropolar Material Model. *Struct. Multidiscip. Optim.* **2017**, *55*, 1–12. [CrossRef]
126. Wang, Z.-P.; Poh, L.H.; Dirrenberger, J.; Zhu, Y.; Forest, S. Isogeometric Shape Optimization of Smoothed Petal Auxetic Structures via Computational Periodic Homogenization. *Comput. Methods Appl. Mech. Engrg.* **2017**, *323*, 250–271. [CrossRef]
127. Gohar, S.; Hussain, G.; Ilyas, M.; Ali, A. Performance of 3D Printed Topologically Optimized Novel Auxetic Structures under Compressive Loading: Experimental and FE Analyses. *J. Mater. Res. Technol.* **2021**, *15*, 394–408. [CrossRef]
128. Harkati, E.; Daoudi, N.; Bezazi, A.; Haddad, A.; Scarpa, F. In-Plane Elasticity of a Multi Re-Entrant Auxetic Honeycomb. *Compos. Struct.* **2017**, *180*, 130–139. [CrossRef]
129. Li, Z.Y.; Wang, X.T.; Ma, L.; Wu, L.Z. Study on the Mechanical Properties of CFRP Composite Auxetic Structures Consist of Corrugated Sheets and Tubes. *Compos. Struct.* **2022**, *292*, 115655. [CrossRef]
130. Lee, J.H.; Choi, J.B.; Choi, K. Application of Homogenization FEM Analysis to Regular and Re-Entrant Honeycomb Structures. *J. Mater. Sci.* **1996**, *31*, 4105–4110. [CrossRef]
131. Zied, K.; Osman, M.; Elmahdy, T. Enhancement of the In-Plane Stiffness of the Hexagonal Re-Entrant Auxetic Honeycomb Cores. *Phys. Status Solidi* **2015**, *252*, 2685–2692. [CrossRef]
132. Usta, F.; Türkmen, H.S.; Scarpa, F. Low-Velocity Impact Resistance of Composite Sandwich Panels with Various Types of Auxetic and Non-Auxetic Core Structures. *Thin-Walled Struct.* **2021**, *163*, 107738. [CrossRef]
133. Usta, F.; Türkmen, H.S.; Scarpa, F. High-Velocity Impact Resistance of Doubly Curved Sandwich Panels with Re-Entrant Honeycomb and Foam Core. *Int. J. Impact Eng.* **2022**, *165*, 104230. [CrossRef]
134. Yang, H.; Wang, B.; Ma, L. Mechanical Properties of 3D Double-U Auxetic Structures. *Int. J. Solids Struct.* **2019**, *180–181*, 13–29. [CrossRef]

135. Bezazi, A.; Scarpa, F.; Remillat, C. A Novel Centresymmetric Honeycomb Composite Structure. *Compos. Struct.* **2005**, *71*, 356–364. [CrossRef]

136. Chen, Y.; Fu, M.; Hu, H.; Xiong, J. Curved Inserts in Auxetic Honeycomb for Property Enhancement and Design Flexibility. *Compos. Struct.* **2022**, *280*, 114892. [CrossRef]

137. Etemadi, E.; Gholikord, M.; Zeeshan, M.; Hu, H. Improved Mechanical Characteristics of New Auxetic Structures Based on Stretch-Dominated-Mechanism Deformation under Compressive and Tensile Loadings. *Thin-Walled Struct.* **2023**, *184*, 110491. [CrossRef]

138. Xu, N.; Liu, H.; An, M.; Wang, L. Novel 2D Star-Shaped Honeycombs with Enhanced Effective Young's Modulus and Negative Poisson's Ratio. *Extrem. Mech. Lett.* **2021**, *43*, 101164. [CrossRef]

139. Zhu, Y.; Luo, Y.; Gao, D.; Yu, C.; Ren, X.; Zhang, C. In-Plane Elastic Properties of a Novel Re-Entrant Auxetic Honeycomb with Zigzag Inclined Ligaments. *Eng. Struct.* **2022**, *268*, 114788. [CrossRef]

140. Lu, Z.; Li, X.; Yang, Z.; Xie, F. Novel Structure with Negative Poisson's Ratio and Enhanced Young's Modulus. *Compos. Struct.* **2016**, *138*, 243–252. [CrossRef]

141. Huang, J.; Zhang, Q.; Scarpa, F.; Liu, Y.; Leng, J. In-Plane Elasticity of a Novel Auxetic Honeycomb Design. *Compos. Part B-Eng.* **2017**, *110*, 72–82. [CrossRef]

142. Mustahsan, F.; Khan, S.Z.; Zaidi, A.A.; Alahmadi, Y.H.; Mahmoud, E.R.I.; Almohamadi, H. Re-Entrant Honeycomb Auxetic Structure with Enhanced Directional Properties. *Materials* **2022**, *15*, 8022. [CrossRef] [PubMed]

143. Guo, M.F.; Yang, H.; Ma, L. Design and Analysis of 2D Double-U Auxetic Honeycombs. *Thin-Walled Struct.* **2020**, *155*, 106915. [CrossRef]

144. Wang, W.; Zhang, W.; Guo, M.; Yang, J.; Ma, L. Energy Absorption Characteristics of a Lightweight Auxetic Honeycomb under Low-Velocity Impact Loading. *Thin-Walled Struct.* **2023**, *185*, 110577. [CrossRef]

145. Zhang, W.; Zhao, S.; Scarpa, F.; Wang, J.; Sun, R. In-Plane Mechanical Behavior of Novel Auxetic Hybrid Metamaterials. *Thin-Walled Struct.* **2021**, *159*, 107191. [CrossRef]

146. Zhan, C.; Li, M.; Mccoy, R.; Zhao, L.; Lu, W. 3D Printed Hierarchical Re-Entrant Honeycombs: Enhanced Mechanical Properties and the Underlying Deformation Mechanisms. *Compos. Struct.* **2022**, *290*, 115550. [CrossRef]

147. Lakes, R.S. Deformation Mechanisms in Negative Poisson's Ratio Materials: Structural Aspects. *J. Mater. Sci.* **1991**, *26*, 2287–2292. [CrossRef]

148. Prall, D.; Lakes, R.S. Properties of a Chiral Honeycomb with a Poisson's Ratio of −1. *Int. J. Mech. Sci.* **1997**, *39*, 305–314. [CrossRef]

149. Alomarah, A.; Ruan, D.; Masood, S. Tensile Properties of an Auxetic Structure with Re-Entrant and Chiral Features—A Finite Element Study. *Int. J. Adv. Manuf. Technol.* **2018**, *99*, 2425–2440. [CrossRef]

150. Attard, D.; Farrugia, P.S.; Gatt, R.; Grima, J.N. Starchirals—A Novel Class of Auxetic Hierarchal Structures. *Int. J. Mech. Sci.* **2020**, *179*, 105631. [CrossRef]

151. Gang, X.; Ren, X.; Jiang, W.; Yu, X.; Luo, C.; Zhang, Y.; Min, Y. A Novel Auxetic Chiral Lattice Composite: Experimental and Numerical Study. *Compos. Struct.* **2022**, *282*, 115043. [CrossRef]

152. Gao, D.; Wang, S.; Zhang, M.; Zhang, C. Experimental and Numerical Investigation on In-Plane Impact Behaviour of Chiral Auxetic Structure. *Compos. Struct.* **2021**, *267*, 113922. [CrossRef]

153. Nečemer, B.; Glodež, S.; Novak, N.; Kramberger, J. Numerical Modelling of a Chiral Auxetic Cellular Structure under Multiaxial Loading Conditions. *Theor. Appl. Fract. Mech.* **2020**, *107*, 102514. [CrossRef]

154. Qi, C.; Jiang, F.; Yu, C.; Yang, S. In-Plane Crushing Response of Tetra-Chiral Honeycombs. *Int. J. Impact Eng.* **2019**, *130*, 247–265. [CrossRef]

155. Shim, J.; Shan, S.; Košmrlj, A.; Kang, S.H.; Chen, E.R.; Weaver, J.C.; Bertoldi, K. Harnessing Instabilities for Design of Soft Reconfigurable Auxetic/Chiral Materials. *Soft Matter* **2013**, *9*, 8198–8202. [CrossRef]

156. Zhang, K.; Zhao, P.; Zhao, C.; Hong, F.; Deng, Z. Study on the Mechanism of Band Gap and Directional Wave Propagation of the Auxetic Chiral Lattices. *Compos. Struct.* **2020**, *238*, 111952. [CrossRef]

157. Gatt, R.; Brincat, J.P.; Azzopardi, K.M.; Mizzi, L.; Grima, J.N. On the Effect of the Mode of Connection between the Node and the Ligaments in Anti-Tetrachiral Systems. *Adv. Eng. Mater.* **2015**, *17*, 189–198. [CrossRef]

158. Mizzi, L.; Attard, D.; Gatt, R.; Pozniak, A.A.; Wojciechowski, K.W.; Grima, J.N. Influence of Translational Disorder on the Mechanical Properties of Hexachiral Honeycomb Systems. *Compos. Part B Eng.* **2015**, *80*, 84–91. [CrossRef]

159. Mizzi, L.; Attard, D.; Gatt, R.; Farrugia, P.S.; Grima, J.N. An Analytical and Finite Element Study on the Mechanical Properties of Irregular Hexachiral Honeycombs. *Smart Mater. Struct.* **2018**, *27*, 105016. [CrossRef]

160. Mizzi, L.; Attard, D.; Gatt, R.; Dudek, K.K.; Ellul, B.; Grima, J.N. Implementation of Periodic Boundary Conditions for Loading of Mechanical Metamaterials and Other Complex Geometric Microstructures Using Finite Element Analysis. *Eng. Comput.* **2021**, *37*, 1765–1779. [CrossRef]

161. Grima, J.N.; Gatt, R. Perforated Sheets Exhibiting Negative Poisson's Ratios. *Adv. Eng. Mater.* **2010**, *12*, 460–464. [CrossRef]

162. Grima, J.; Mizzi, L.; Azzopardi, K.M.; Gatt, R. Auxetic Perforated Mechanical Metamaterials with Randomly Oriented Cuts. *Adv. Mater.* **2016**, *28*, 385–389. [CrossRef] [PubMed]

163. Mizzi, L.; Azzopardi, K.M.; Attard, D.; Grima, J.N.; Gatt, R. Auxetic Metamaterials Exhibiting Giant Negative Poisson's Ratios. *Phys. Status Solidi—Rapid Res. Lett.* **2015**, *9*, 425–430. [CrossRef]

164. Grima, J.N.; Gatt, R.; Ellul, B.; Chetcuti, E. Auxetic Behaviour in Non-Crystalline Materials Having Star or Triangular Shaped Perforations. *J. Non-Cryst. Solids* **2010**, *356*, 1980–1987. [CrossRef]

165. Mizzi, L.; Attard, D.; Evans, K.E.; Gatt, R.; Grima, J.N. Auxetic Mechanical Metamaterials with Diamond and Elliptically Shaped Perforations. *Acta Mech.* **2021**, *232*, 779–791. [CrossRef]

166. Billon, K.; Zampetakis, I.; Scarpa, F.; Ouisse, M.; Sadoulet-Reboul, E.; Collet, M.; Perriman, A.; Hetherington, A. Mechanics and Band Gaps in Hierarchical Auxetic Rectangular Perforated Composite Metamaterials. *Compos. Struct.* **2017**, *160*, 1042–1050. [CrossRef]

167. Yao, J.; Sun, R.; Scarpa, F.; Remillat, C.; Gao, Y.; Su, Y. Two-Dimensional Graded Metamaterials with Auxetic Rectangular Perforations. *Compos. Struct.* **2021**, *261*, 113313. [CrossRef]

168. Grima, J.N.; Evans, K.E. Auxetic Behavior from Rotating Squares. *J. Mater. Sci. Lett.* **2000**, *19*, 1563–1565. [CrossRef]

169. Grima, J.N.; Evans, K.E. Auxetic Behavior from Rotating Triangles. *J. Mater. Sci.* **2006**, *41*, 3193–3196. [CrossRef]

170. Wang, H.; Xiao, S.; Wang, J. Disordered Auxetic Metamaterials Architected by Random Peanut-Shaped Perturbations. *Mater. Des.* **2021**, *212*, 110291. [CrossRef]

171. Atilla Yolcu, D.; Okutan Baba, B. Measurement of Poisson's Ratio of the Auxetic Structure. *Meas. J. Int. Meas. Confed.* **2022**, *204*, 112040. [CrossRef]

172. Acuna, D.; Gutiérrez, F.; Silva, R.; Palza, H.; Nunez, A.S.; Düring, G. A Three Step Recipe for Designing Auxetic Materials on Demand. *Commun. Phys.* **2022**, *5*, 1–9. [CrossRef]

173. Mrozek, A.; Strek, T. Numerical Analysis of Dynamic Properties of an Auxetic Structure with Rotating Squares with Holes. *Materials* **2022**, *15*, 8712. [CrossRef] [PubMed]

174. Chetcuti, E.; Ellul, B.; Manicaro, E.; Brincat, J.P.J.-P.; Attard, D.; Gatt, R.; Grima, J.N. Modeling Auxetic Foams through Semi-Rigid Rotating Triangles. *Phys. Status Solidi* **2014**, *251*, 297–306. [CrossRef]

175. Grima-Cornish, J.N.; Grima, J.N.; Attard, D. Negative Mechanical Materials and Metamaterials: Giant Out-of-Plane Auxeticity from Multi-Dimensional Wine-Rack-like Motifs. *MRS Adv.* **2020**, *5*, 717–725. [CrossRef]

176. Hur, J.M.; Seo, D.S.; Kim, K.; Lee, J.K.; Lee, K.J.; Kim, Y.Y.; Kim, D.N. Harnessing Distinct Deformation Modes of Auxetic Patterns for Stiffness Design of Tubular Structures. *Mater. Des.* **2021**, *198*, 109376. [CrossRef]

177. Mizzi, L.; Gatt, R.; Grima, J.N. Non-Porous Grooved Single-Material Auxetics. *Phys. Status Solidi* **2015**, *252*, 1559–1564. [CrossRef]

178. Grima, J.N.; Jackson, R.; Alderson, A.; Evans, K.E. Do Zeolites Have Negative Poisson's Ratios? *Adv. Mater.* **2000**, *12*, 1912–1918. [CrossRef]

179. Alderson, A.; Alderson, K.L.; Evans, K.E.; Grima, J.N.; Williams, M.R.; Davies, P.J. Modelling the Deformation Mechanisms, Structure-Property Relationships and Applications of Auxetic Nanomaterials. *Phys. Status Solidi Basic Res.* **2005**, *242*, 499–508. [CrossRef]

180. Grima-Cornish, J.N.; Vella-Żarb, L.; Grima, J.N.; Evans, K.E. Boron Arsenate and Its Pressure-Dependent Auxetic Properties. *APL Mater.* **2022**, *10*, 091109. [CrossRef]

181. Hoberman, C. Reversibly Expandable Doubly-Curved Truss Structure. U.S. Patent 4,942,700, 24 July 1990.

182. Alderson, A.; Alderson, K.L.; Chirima, G.; Ravirala, N.; Zied, K.M. The In-Plane Linear Elastic Constants and out-of-Plane Bending of 3-Coordinated Ligament and Cylinder-Ligament Honeycombs. *Compos. Sci. Technol.* **2010**, *70*, 1034–1041. [CrossRef]

183. Grima, J.N.; Cauchi, R.; Gatt, R.; Attard, D. Honeycomb Composites with Auxetic Out-of-Plane Characteristics. *Compos. Struct.* **2013**, *106*, 150–159. [CrossRef]

184. Lyngdoh, G.A.; Kelter, N.K.; Doner, S.; Krishnan, N.M.A.; Das, S. Elucidating the Auxetic Behavior of Cementitious Cellular Composites Using Finite Element Analysis and Interpretable Machine Learning. *Mater. Des.* **2022**, *213*, 110341. [CrossRef]

185. Poźniak, A.A.A.; Wojciechowski, K.W.; Grima, J.N.; Mizzi, L. Planar Auxeticity from Elliptic Inclusions. *Compos. Part B Eng.* **2016**, *94*, 379–388. [CrossRef]

186. Roche, J.; Von Lockette, P.; Lofland, S. Study of Hard-and Soft-Magnetorheological Elastomers (MRE's) Actuation Capabilities. In *Proceedings of the 2011 COMSOL Conference in Boston*; COMSOL, Inc.: Burlington, MA, USA, 2011.

187. Li, Z.-Y.Y.; Wang, X.-T.T.; Ma, L.; Wu, L.-Z.Z.; Wang, L. Auxetic and Failure Characteristics of Composite Stacked Origami Cellular Materials under Compression. *Thin-Walled Struct.* **2023**, *184*, 110453. [CrossRef]

188. Changfang, Z.; Changlin, Z.; Jianlin, Z.; Hongwei, Z.; Kebin, Z.; Yangzuo, L. Compressive Mechanical Behavior for Surface Auxetic Structures. *J. Alloys Compd.* **2022**, *894*, 162427. [CrossRef]

189. Yang, L.; Harrysson, O.; West, H.; Cormier, D. Mechanical Properties of 3D Re-Entrant Honeycomb Auxetic Structures Realized via Additive Manufacturing. *Int. J. Solids Struct.* **2015**, *69–70*, 475–490. [CrossRef]

190. Wang, X.T.; Li, X.W.; Ma, L. Interlocking Assembled 3D Auxetic Cellular Structures. *Mater. Des.* **2016**, *99*, 467–476. [CrossRef]

191. Wang, X.-T.; Wang, B.; Li, X.; Ma, L. Mechanical Properties of 3D Re-Entrant Auxetic Cellular Structures. *Int. J. Mech. Sci.* **2017**, *131–132*, 396–407. [CrossRef]

192. Nasim, M.S.; Etemadi, E. Three Dimensional Modeling of Warp and Woof Periodic Auxetic Cellular Structure. *Int. J. Mech. Sci.* **2018**, *136*, 475–481. [CrossRef]

193. Farrugia, P.S.; Gatt, R.; Grima, J.N. A Novel Three-Dimensional Anti-Tetrachiral Honeycomb. *Phys. Status Solidi Basic Res.* **2019**, *256*, 1800473. [CrossRef]

194. Wang, Q.; Yang, Z.; Lu, Z.; Li, X. Mechanical Responses of 3D Cross-Chiral Auxetic Materials under Uniaxial Compression. *Mater. Des.* **2020**, *186*, 108226. [CrossRef]

195. Grima, J.N.; Zammit, V.; Gatt, R.; Alderson, A.; Evans, K.E. Auxetic Behaviour from Rotating Semi-Rigid Units. *Phys. Status Solidi* **2007**, *244*, 866–882. [CrossRef]

196. Photiou, D.; Avraam, S.; Sillani, F.; Verga, F.; Jay, O.; Papadakis, L. Experimental and Numerical Analysis of 3D Printed Polymer Tetra-Petal Auxetic Structures under Compression. *Appl. Sci.* **2021**, *11*, 10362. [CrossRef]

197. Grima-Cornish, J.N.; Attard, D.; Vella-Żarb, L.; Grima, J.N.; Evans, K.E. Boron Arsenate Scaled-Up: An Enhanced Nano-Mimicking Mechanical Metamaterial. *Phys. Status Solidi Basic Res.* **2022**, *259*, 1–12. [CrossRef]

198. Galea, R.; Farrugia, P.-S.; Dudek, K.K.; Attard, D.; Grima, J.N.; Gatt, R. A Novel Design Method to Produce 3D Auxetic Metamaterials with Continuous Pores Exemplified through 3D Rotating Auxetic Systems. *Mater. Des.* **2023**, *226*, 111596. [CrossRef]

199. Su, Y.; Xu, X.; Shi, J.; Huang, G. A 3D Mechanism-Driven Hexagonal Metamaterial: Evaluation of Auxetic Behavior. *Int. J. Mech. Sci.* **2021**, *209*, 106699. [CrossRef]

200. Gatt, R.; Mizzi, L.; Azzopardi, J.I.; Azzopardi, K.M.; Attard, D.; Casha, A.; Briffa, J.; Grima, J.N. Hierarchical Auxetic Mechanical Metamaterials. *Sci. Rep.* **2015**, *5*, 8395. [CrossRef] [PubMed]

201. Wan, M.; Yu, K.; Sun, H. 4D Printed Programmable Auxetic Metamaterials with Shape Memory Effects. *Compos. Struct.* **2022**, *279*, 114791. [CrossRef]

202. Gao, Q.; Zhao, X.; Wang, C.; Wang, L.; Ma, Z. Multi-Objective Crashworthiness Optimization for an Auxetic Cylindrical Structure under Axial Impact Loading. *Mater. Des.* **2018**, *143*, 120–130. [CrossRef]

203. Peng, X.L.; Soyarslan, C.; Bargmann, S. Phase Contrast Mediated Switch of Auxetic Mechanism in Composites of Infilled Re-Entrant Honeycomb Microstructures. *Extrem. Mech. Lett.* **2020**, *35*, 100641. [CrossRef]

204. Han, D.; Zhang, Y.; Yu, X.; Min, Y.; Ren, X. Mechanical Characterization of a Novel Thickness Gradient Auxetic Tubular Structure under Inclined Load. *Eng. Struct.* **2022**, *273*, 115079. [CrossRef]

205. Han, D.; Ren, X.; Zhang, Y.; Yu Zhang, X.; Gang Zhang, X.; Luo, C.; Min Xie, Y. Lightweight Auxetic Metamaterials: Design and Characteristic Study. *Compos. Struct.* **2022**, *293*, 115706. [CrossRef]

206. Chen, Z.; Wu, X.; Min, Y.; Wang, Z.; Zhou, S. Re-Entrant Auxetic Lattices with Enhanced Stiffness: A Numerical Study. *Int. J. Mech. Sci.* **2020**, *178*, 105619. [CrossRef]

207. Novak, N.; Vesenjak, M.; Tanaka, S.; Hokamoto, K.; Ren, Z. Compressive Behaviour of Chiral Auxetic Cellular Structures at Diferent Strain Rates. *Int. J. Impact Eng.* **2020**, *141*, 103566. [CrossRef]

208. Liu, J.; Liu, H. Energy Absorption Characteristics and Stability of Novel Bionic Negative Poisson's Ratio Honeycomb under Oblique Compression. *Eng. Struct.* **2022**, *267*, 114682. [CrossRef]

209. Logakannan, K.P.; Ramachandran, V.; Rengaswamy, J.; Gao, Z.; Ruan, D. Quasi-Static and Dynamic Compression Behaviors of a Novel Auxetic Structure. *Compos. Struct.* **2020**, *254*, 112853. [CrossRef]

210. Jiang, H.; Ren, Y.; Jin, Q.; Zhu, G.; Hu, Y.; Cheng, F. Crashworthiness of Novel Concentric Auxetic Reentrant Honeycomb with Negative Poisson's Ratio Biologically Inspired by Coconut Palm. *Thin-Walled Struct.* **2020**, *154*, 106911. [CrossRef]

211. Tan, H.L.; He, Z.C.; Li, K.X.; Li, E.; Cheng, A.G.; Xu, B. In-Plane Crashworthiness of Re-Entrant Hierarchical Honeycombs with Negative Poisson's Ratio. *Compos. Struct.* **2019**, *229*, 111415. [CrossRef]

212. Lu, H.; Wang, X.; Chen, T. In-Plane Dynamics Crushing of a Combined Auxetic Honeycomb with Negative Poisson's Ratio and Enhanced Energy Absorption. *Thin-Walled Struct.* **2021**, *160*, 107366. [CrossRef]

213. Li, Z.; Gao, Q.; Yang, S.; Wang, L.; Tang, J. Comparative Study of the In-Plane Uniaxial and Biaxial Crushing of Hexagonal, Re-Entrant, and Mixed Honeycombs. *J. Sandw. Struct. Mater.* **2019**, *21*, 1991–2013. [CrossRef]

214. Qi, C.; Jiang, F.; Yang, S.; Remennikov, A. Multi-Scale Characterization of Novel Re-Entrant Circular Auxetic Honeycombs under Quasi-Static Crushing. *Thin-Walled Struct.* **2021**, *169*, 108314. [CrossRef]

215. Wei, L.; Zhao, X.; Yu, Q.; Zhu, G. A Novel Star Auxetic Honeycomb with Enhanced In-Plane Crushing Strength. *Thin-Walled Struct.* **2020**, *149*, 106623. [CrossRef]

216. Singh, R.; Javanbakht, Z.; Hall, W. On the Inclined Static Loading of Honeycomb Re-Entrant Auxetics. *Compos. Struct.* **2021**, *273*, 114289. [CrossRef]

217. Dhari, R.S.; Javanbakht, Z.; Hall, W. On the Deformation Mechanism of Re-Entrant Honeycomb Auxetics under Inclined Static Loads. *Mater. Lett.* **2021**, *286*, 129214. [CrossRef]

218. Wang, T.; Li, Z.; Wang, L.; Ma, Z.; Hulbert, G.M. Dynamic Crushing Analysis of a Three-Dimensional Re-Entrant Auxetic Cellular Structure. *Materials* **2019**, *12*, 460. [CrossRef]

219. Liu, W.; Wang, N.; Luo, T.; Lin, Z. In-Plane Dynamic Crushing of Re-Entrant Auxetic Cellular Structure. *Mater. Des.* **2016**, *100*, 84–91. [CrossRef]

220. Ou, Y.; Yan, S.; Wen, P. In-Plane Impact Dynamics Analysis of Re-Entrant Honeycomb with Variable Cross-Section. *Comput. Model. Eng. Sci.* **2021**, *127*, 209–222. [CrossRef]

221. Hu, L.L.; Zhou, M.Z.; Deng, H. Dynamic Indentation of Auxetic and Non-Auxetic Honeycombs under Large Deformation. *Compos. Struct.* **2019**, *207*, 323–330. [CrossRef]

222. Li, T.; Liu, F.; Wang, L. Enhancing Indentation and Impact Resistance in Auxetic Composite Materials. *Compos. Part B Eng.* **2020**, *198*, 108229. [CrossRef]

223. Krushynska, A.O.; Torrent, D.; Aragón, A.M.; Ardito, R.; Bilal, O.R.; Bonello, B.; Bosia, F.; Chen, Y.; Christensen, J.; Colombi, A.; et al. Emerging Topics in Nanophononics and Elastic, Acoustic, and Mechanical Metamaterials: An Overview. *Nanophotonics* **2023**, *12*, 659–686. [CrossRef]

224. Mei, J.; Ma, G.; Yang, M.; Yang, Z.; Wen, W.; Sheng, P. Dark Acoustic Metamaterials as Super Absorbers for Low-Frequency Sound. *Nat. Commun.* **2012**, *3*, 756. [CrossRef]

225. Tang, Y.; Ren, S.; Meng, H.; Xin, F.; Huang, L.; Chen, T.; Zhang, C.; Lu, T.J. Hybrid Acoustic Metamaterial as Super Absorber for Broadband Low-Frequency Sound. *Sci. Rep.* **2017**, *7*, 43340. [CrossRef] [PubMed]

226. Cummer, S.A.; Christensen, J.; Alù, A. Controlling Sound with Acoustic Metamaterials. *Nat. Rev. Mater.* **2016**, *1*, 16001. [CrossRef]

227. Christensen, J.; de Abajo, F.J.G. Anisotropic Metamaterials for Full Control of Acoustic Waves. *Phys. Rev. Lett.* **2012**, *108*, 124301. [CrossRef]

228. Achaoui, Y.; Ungureanu, B.; Enoch, S.; Brûlé, S.; Guenneau, S. Seismic Waves Damping with Arrays of Inertial Resonators. *Extrem. Mech. Lett.* **2016**, *8*, 30–37. [CrossRef]

229. Brûlé, S.; Javelaud, E.H.; Enoch, S.; Guenneau, S. Experiments on Seismic Metamaterials: Molding Surface Waves. *Phys. Rev. Lett.* **2014**, *112*, 133901. [CrossRef] [PubMed]

230. Colombi, A.; Colquitt, D.; Roux, P.; Guenneau, S.; Craster, R. V A Seismic Metamaterial: The Resonant Metawedge. *Sci. Rep.* **2016**, *6*, 27717. [CrossRef] [PubMed]

231. Krödel, S.; Thomé, N.; Daraio, C. Wide Band-Gap Seismic Metastructures. *Extrem. Mech. Lett.* **2015**, *4*, 111–117. [CrossRef]

232. De Ponti, J.M.; Colombi, A.; Ardito, R.; Braghin, F.; Corigliano, A.; Craster, R. V Graded Elastic Metasurface for Enhanced Energy Harvesting. *New J. Phys.* **2020**, *22*, 13013. [CrossRef]

233. Jensen, J.S. Phononic Band Gaps and Vibrations in One- and Two-Dimensional Mass–Spring Structures. *J. Sound Vib.* **2003**, *266*, 1053–1078. [CrossRef]

234. Li, L.; Ruan, H.; Liu, C.; Li, Y.; Shuang, Y.; Alù, A.; Qiu, C.-W.; Cui, T.J. Machine-Learning Reprogrammable Metasurface Imager. *Nat. Commun.* **2019**, *10*, 1082. [CrossRef]

235. Coulombe, J.C.; York, M.C.A.; Sylvestre, J. Computing with Networks of Nonlinear Mechanical Oscillators. *PLoS ONE* **2017**, *12*, e0178663. [CrossRef]

236. Milton, G.W. *The Theory of Composites*; Cambridge University Press: Cambridge, UK, 2002.

237. Hussein, M.I.; Leamy, M.J.; Ruzzene, M. Dynamics of Phononic Materials and Structures: Historical Origins, Recent Progress, and Future Outlook. *Appl. Mech. Rev.* **2014**, *66*, 040802. [CrossRef]

238. Khelif, A.; Aoubiza, B.; Mohammadi, S.; Adibi, A.; Laude, V. Complete Band Gaps in Two-Dimensional Phononic Crystal Slabs. *Phys. Rev. E* **2006**, *74*, 46610. [CrossRef]

239. Baravelli, E.; Ruzzene, M. Internally Resonating Lattices for Bandgap Generation and Low-Frequency Vibration Control. *J. Sound Vib.* **2013**, *332*, 6562–6579. [CrossRef]

240. Süsstrunk, R.; Huber, S.D. Classification of Topological Phonons in Linear Mechanical Metamaterials. *Proc. Natl. Acad. Sci. USA* **2016**, *113*, E4767–E4775. [CrossRef]

241. Chaplain, G.J.; De Ponti, J.M.; Aguzzi, G.; Colombi, A.; Craster, R. V Topological Rainbow Trapping for Elastic Energy Harvesting in Graded Su-Schrieffer-Heeger Systems. *Phys. Rev. Appl.* **2020**, *14*, 54035. [CrossRef]

242. Khanikaev, A.B.; Fleury, R.; Mousavi, S.H.; Alù, A. Topologically Robust Sound Propagation in an Angular-Momentum-Biased Graphene-like Resonator Lattice. *Nat. Commun.* **2015**, *6*, 8260. [CrossRef] [PubMed]

243. Krushynska, A.O.; Miniaci, M.; Bosia, F.; Pugno, N.M. Coupling Local Resonance with Bragg Band Gaps in Single-Phase Mechanical Metamaterials. *Extrem. Mech. Lett.* **2017**, *12*, 30–36. [CrossRef]

244. Lu, M.-H.; Feng, L.; Chen, Y.-F. Phononic Crystals and Acoustic Metamaterials. *Mater. Today* **2009**, *12*, 34–42. [CrossRef]

245. Robillard, J.F.; Matar, O.B.; Vasseur, J.O.; Deymier, P.A.; Stippinger, M.; Hladky-Hennion, A.C.; Pennec, Y.; Djafari-Rouhani, B. Tunable Magnetoelastic Phononic Crystals. *Appl. Phys. Lett.* **2009**, *95*, 124104. [CrossRef]

246. Chen, Y.; Kadic, M.; Wegener, M. Roton-like Acoustical Dispersion Relations in 3D Metamaterials. *Nat. Commun.* **2021**, *12*, 3278. [CrossRef] [PubMed]

247. Zheludev, N.I.; Kivshar, Y.S. From Metamaterials to Metadevices. *Nat. Mater.* **2012**, *11*, 917–924. [CrossRef]

248. Iglesias Martínez, J.A.; Moughames, J.; Ulliac, G.; Kadic, M.; Laude, V. Three-Dimensional Phononic Crystal with Ultra-Wide Bandgap at Megahertz Frequencies. *Appl. Phys. Lett.* **2021**, *118*, 063507. [CrossRef]

249. Craster, R.V.; Guenneau, S. *Acoustic Metamaterials*; Craster, R.V., Guenneau, S., Eds.; SSMaterial; Springer: Dordrecht, The Netherlands, 2012; ISBN 978-94-007-9467-2.

250. D'Alessandro, L.; Belloni, E.; Ardito, R.; Corigliano, A.; Braghin, F. Modeling and Experimental Verification of an Ultra-Wide Bandgap in 3D Phononic Crystal. *Appl. Phys. Lett.* **2016**, *109*, 2–6. [CrossRef]

251. Warmuth, F.; Wormser, M.; Körner, C. Single Phase 3D Phononic Band Gap Material. *Sci. Rep.* **2017**, *7*, 3843. [CrossRef] [PubMed]

252. Lucklum, F.; Vellekoop, M.J. Bandgap Engineering of Three-Dimensional Phononic Crystals in a Simple Cubic Lattice. *Appl. Phys. Lett.* **2018**, *113*, 201902. [CrossRef]

253. Liu, Z.; Zhang, X.; Mao, Y.; Zhu, Y.Y.; Yang, Z.; Chan, C.T.; Sheng, P. Locally Resonant Sonic Materials. *Science* **2000**, *289*, 1734–1736. [CrossRef]

254. Mu, D.; Shu, H.; Zhao, L.; An, S. A Review of Research on Seismic Metamaterials. *Adv. Eng. Mater.* **2020**, *22*, 1901148. [CrossRef]

255. Oudich, M.; Gerard, N.J.R.K.; Deng, Y.; Jing, Y. Tailoring Structure-Borne Sound through Bandgap Engineering in Phononic Crystals and Metamaterials: A Comprehensive Review. *Adv. Funct. Mater.* **2023**, *33*, 35–39. [CrossRef]

256. Kunin, V.; Yang, S.; Cho, Y.; Deymier, P.; Srolovitz, D.J. Static and Dynamic Elastic Properties of Fractal-Cut Materials. *Extrem. Mech. Lett.* **2016**, *6*, 103–114. [CrossRef]

257. Huang, Y.; Li, J.; Chen, W.; Bao, R. Tunable Bandgaps in Soft Phononic Plates with Spring-Mass-like Resonators. *Int. J. Mech. Sci.* **2019**, *151*, 300–313. [CrossRef]

258. Bertoldi, K.; Boyce, M.C. Wave Propagation and Instabilities in Monolithic and Periodically Structured Elastomeric Materials Undergoing Large Deformations. *Phys. Rev. B* **2008**, *78*, 184107. [CrossRef]

259. Bertoldi, K.; Boyce, M.C. Mechanically Triggered Transformations of Phononic Band Gaps in Periodic Elastomeric Structures. *Phys. Rev. B* **2008**, *77*, 52105. [CrossRef]

260. Dudek, K.K.; Iglesias Martínez, J.A.; Ulliac, G.; Hirsinger, L.; Wang, L.; Laude, V.; Kadic, M. Micro-Scale Mechanical Metamaterial with a Controllable Transition in the Poisson's Ratio and Band Gap Formation. *Adv. Mater.* **2023**, *35*, 65–69. [CrossRef]

261. Zhang, H.; Cheng, X.; Yan, D.; Zhang, Y.; Fang, D. A Nonlinear Mechanics Model of Soft Network Metamaterials with Unusual Swelling Behavior and Tunable Phononic Band Gaps. *Compos. Sci. Technol.* **2019**, *183*, 107822. [CrossRef]

262. Hu, W.; Ren, Z.; Wan, Z.; Qi, D.; Cao, X.; Li, Z.; Wu, W.; Tao, R.; Li, Y. Deformation Behavior and Band Gap Switching Function of 4D Printed Multi-Stable Metamaterials. *Mater. Des.* **2021**, *200*, 109481. [CrossRef]

263. Nimmagadda, C.; Matlack, K.H. Thermally Tunable Band Gaps in Architected Metamaterial Structures. *J. Sound Vib.* **2019**, *439*, 29–42. [CrossRef]

264. Chen, Y.; Li, T.; Scarpa, F.; Wang, L. Lattice Metamaterials with Mechanically Tunable Poisson's Ratio for Vibration Control. *Phys. Rev. Appl.* **2017**, *7*, 24012. [CrossRef]

265. Chow, L.; Yick, K.L.; Wong, K.H.; Leung, M.S.; Sun, Y.; Kwan, M.; Ning, K.; Yu, A.; Yip, J.; Chan, Y.; et al. 3D Printing Auxetic Architectures for Hypertrophic Scar Therapy. *Macromol. Mater. Eng.* **2022**, *307*, 2100866. [CrossRef]

266. Menon, H.G.; Dutta, S.; Krishnan, A.; Hariprasad, M.P. Proposed Auxetic Cluster Designs for Lightweight Structural Beams with Improved Load Bearing Capacity. *Eng. Struct.* **2022**, *260*, 114241. [CrossRef]

267. Sadegh, M.; Ranjbar, M.; Boldrin, L.; Scarpa, F.; Patsias, S.; Ozada, N. Vibroacoustics of 2D Gradient Auxetic Hexagonal Honeycomb Sandwich Panels. *Compos. Struct.* **2018**, *187*, 593–603. [CrossRef]

268. Jianbao, L.; Wang, Y.S.; Zhang, C. Finite Element Method for Analysis of Band Structures of Three Dimensonal Phononic Crystals. In Proceedings of the 2008 IEEE Ultrasonics Symposium, Beijing, China, 2–5 November 2008; pp. 1468–1471. [CrossRef]

269. Li, J.; Wang, Y.S.; Zhang, C. Finite Element Method for Analysis of Band Structures of Phononic Crystal Slabs with Archimedean-like Tilings. In Proceedings of the 2009 IEEE International Ultrasonics Symposium, Rome, Italy, 20–23 September 2009; pp. 1548–1551. [CrossRef]

270. Koutsianitis, P.I.; Tairidis, G.K.; Drosopoulos, G.A.; Stavroulakis, G.E. Conventional and Star-Shaped Auxetic Materials for the Creation of Band Gaps. *Arch. Appl. Mech.* **2019**, *89*, 2545–2562. [CrossRef]

271. Koutsianitis, P.I.; Tairidis, G.K.; Stavroulakis, G.E. Shunted Piezoelectric Patches on Auxetic Microstructures for the Enhancement of Band Gaps. *Arch. Appl. Mech.* **2021**, *91*, 739–751. [CrossRef]

272. Li, C.; Shen, H.S.; Wang, H.; Yu, Z. Large Amplitude Vibration of Sandwich Plates with Functionally Graded Auxetic 3D Lattice Core. *Int. J. Mech. Sci.* **2020**, *174*, 105472. [CrossRef]

273. Andriya, N.; Dutta, V.; Vani, V.V. Study on 3D Printed Auxetic Structure-Based Non-Pneumatic Tyres (NPT'S). *Mater. Manuf. Process.* **2022**, *37*, 1280–1297. [CrossRef]

274. Wu, T.; Li, M.; Zhu, X.; Lu, X. Research on Non-Pneumatic Tire with Gradient Anti-Tetrachiral Structures. *Mech. Adv. Mater. Struct.* **2021**, *28*, 2351–2359. [CrossRef]

275. Zang, L.; Wang, X.; Yan, P.; Zhao, Z. Structural Design and Characteristics of a Non-Pneumatic Tire with Honeycomb Structure. *Mech. Adv. Mater. Struct.* **2021**, *29*, 4066–4073. [CrossRef]

276. Newton-Mann, C.; Winwood, K.; Driscoll, H.; Hamilton, N.; Allen, T. Finite Element Model of an Impact on a Palmar Pad from a Snowboard Wrist Protector. *Proceedings* **2018**, *2*, 314. [CrossRef]

277. Hernández, S.; Brebbia, C.A.; El-Sayed, M.E.M. Helmet Optimisation Based on Head-Helmet Modelling. *WIT Trans. Built Environ.* **2003**, *67*, 339.

278. Mosleh, Y.; Cajka, M.; Depreitere, B.; Van der Sloten, J.; Ivens, J. Designing Safer Composite Helmets to Reduce Rotational Accelerations during Oblique Impacts. *J. Eng. Med.* **2018**, *232*, 479–491. [CrossRef] [PubMed]

279. Allen, T.; Haake, S.; Goodwill, S. Comparison of a Finite Element Model of a Tennis Racket to Experimental Data. *Sports Eng.* **2009**, *12*, 87–98. [CrossRef]

280. Kays, B.T.; Smith, L.V. Effect of Ice Hockey Stick Stiffness on Performance. *Sports Eng.* **2017**, *20*, 245–254. [CrossRef]

281. Valentini, P.P.; Pennestrì, E.; Quattrociocchi, L. Biomechanical Model for Simulating Impacts against Protective Padding of Sport Facility. *Sports Eng.* **2016**, *19*, 47–57. [CrossRef]

282. Airoldi, A.; Novak, N.; Sgobba, F.; Gilardelli, A.; Borovinšek, M. Foam-Filled Energy Absorbers with Auxetic Behaviour for Localized Impacts. *Mater. Sci. Eng. A* **2020**, *788*, 139500. [CrossRef]

283. Chen, Z.; Li, J.; Wu, B.; Chen, X.; Ren, X.; Xie, Y. A Novel Bio-Inspired Helmet with Auxetic Lattice Liners for Mitigating Traumatic Brain Injury. *Smart Mater. Struct.* **2023**, *32*, 105020. [CrossRef]

284. Easey, N.; Chuprynyuk, D.; Musa, W.M.S.W.; Bangs, A.; Dobah, Y.; Shterenlikht, A.; Scarpa, F. Dome-Shape Auxetic Cellular Metamaterials: Manufacturing, Modeling, and Testing. *Front. Mater.* **2019**, *6*, 86. [CrossRef]

285. Tan, H.; He, Z.; Li, E.; Cheng, A.; Chen, T.; Tan, X.; Li, Q.; Xu, B. Crashworthiness Design and Multi-Objective Optimization of a Novel Auxetic Hierarchical Honeycomb Crash Box. *Struct. Multidiscip. Optim.* **2021**, *64*, 2009–2024. [CrossRef]

286. Nallavan, G. Impact of Recent Developments in Fabrication of Auxetic Materials on Safety and Protection in Sport. *AIP Conf. Proc.* **2020**, *2271*, 030006. [CrossRef]

287. Shepherd, T.; Winwood, K.; Venkatraman, P.; Alderson, A.; Allen, T. Validation of a Finite Element Modeling Process for Auxetic Structures under Impact. *Phys. Status Solidi* **2020**, *257*, 1900197. [CrossRef]

288. Novak, N.; Vesenjak, M.; Kennedy, G.; Thadhani, N.; Ren, Z. Response of Chiral Auxetic Composite Sandwich Panel to Fragment Simulating Projectile Impact. *Phys. Status Solidi* **2019**, *1*, 1900099. [CrossRef]

289. Novak, N.; Starčevič, L.; Vesenjak, M.; Ren, Z. Blast Response Study of the Sandwich Composite Panels with 3D Chiral Auxetic Core. *Compos. Struct.* **2019**, *210*, 167–178. [CrossRef]

290. Wang, Y.; Zhao, W.; Zhou, G.; Wang, C. International Journal of Mechanical Sciences Analysis and Parametric Optimization of a Novel Sandwich Panel with Double-V Auxetic Structure Core under Air Blast Loading. *Int. J. Mech. Sci.* **2018**, *142–143*, 245–254. [CrossRef]

291. Yang, C.; Chang, Y.B.; Lee, D. Nonlinearity of Enhanced Cell Structures Having Auxetic Material Properties. In Proceedings of the ASME International Mechanical Engineering Congress and Exposition, Salt Lake City, UT, USA, 11–14 November 2019; Volume 12. [CrossRef]

292. Chang, Y.; Liu, Y.; Hu, H. A Finite Element Analysis of Auxetic Composite Fabric with Rotating Square Structure. *J. Ind. Text.* **2023**, *53*, 152808372311731. [CrossRef]

293. Lupo, M.; Sofia, D.; Barletta, D.; Poletto, M. Calibration of DEM Simulation of Cohesive Particles. *Chem. Eng. Transect.* **2019**, *74*, 379–384. [CrossRef]